

1

2

3

4 **A ribosome assembly stress response regulates transcription**
5 **to maintain proteome homeostasis**

6

7

8 Benjamin Albert¹, Isabelle C. Kos-Braun², Anthony K. Henras³, Christophe Dez³, Maria Paula Rueda¹,
9 Xu Zhang¹, Olivier Gadal³, Martin Kos², and David Shore^{1*}

10

11 ¹ Department of Molecular Biology and Institute of Genetics and Genomics of Geneva (iGE3), 30 quai
12 Ernest-Ansermet, 1211 Geneva 4, Switzerland

13 ² Heidelberg University Biochemistry Center (BZH), Im Neuenheimer Feld 328, 69120 Heidelberg,
14 Germany

15 ³ Centre de Biologie Intégrative, Université Paul Sabatier, 118 Route de Narbonne, 31062 Toulouse,
16 France

17

18 * Corresponding author: David.Shore@unige.ch

19

20 **Abstract**

21 Ribosome biogenesis is a complex and energy-demanding process requiring tight coordination of
22 ribosomal RNA (rRNA) and ribosomal protein (RP) production. Given the extremely high level of RP
23 synthesis in rapidly growing cells, alteration of any step in the ribosome assembly process may impact
24 growth by leading to proteotoxic stress. Although the transcription factor Hsf1 has emerged as a
25 central regulator of proteostasis, how its activity is coordinated with ribosome biogenesis is unknown.
26 Here we show that arrest of ribosome biogenesis in the budding yeast *S. cerevisiae* triggers rapid
27 activation of a highly specific stress pathway that coordinately up-regulates Hsf1 target genes and
28 down-regulates RP genes. Activation of Hsf1 target genes requires neo-synthesis of RPs, which
29 accumulate in an insoluble fraction and presumably titrate a negative regulator of Hsf1, the Hsp70
30 chaperone. RP aggregation is also coincident with that of the RP gene activator Ifh1, a transcription
31 factor that is rapidly released from RP gene promoters. Our data support a model in which the levels
32 of newly-synthesized RPs, imported into the nucleus but not yet assembled into ribosomes, work to
33 continuously balance Hsf1 and Ifh1 activity, thus guarding against proteotoxic stress during ribosome
34 assembly.
35

36 Introduction

37 Ribosome assembly is the most energy demanding process linked to cell growth and requires
38 coordinated production of processed ribosomal RNAs (rRNAs), ribosomal proteins (RPs) and ribosome
39 biogenesis (RiBi) factors. This massive biosynthetic program permits rapidly growing yeast cells to
40 produce about 2,000 ribosomes per minute [1], which is critical for sustaining high rates of growth
41 (mass accumulation) and proliferation. At the same time, though, ribosome assembly poses a
42 constant threat to cellular protein homeostasis and continued growth, since it requires the
43 coordinated and large-scale assembly of four rRNAs with 79 different RPs, the latter of which are
44 known to be highly prone to aggregation [2-5]. Indeed, unassembled RPs in metazoans have long
45 been known to activate p53, through titration of its negative regulator MDM2, and conserved p53-
46 independent pathways that respond to perturbations in ribosome assembly are now beginning to
47 emerge [6]. Given the absence of p53 in yeasts, *S. cerevisiae* is a promising model system in which to
48 uncover ancestral processes that might monitor ribosome assembly to regulate growth and protein
49 homeostasis in eukaryotes.

50 Heat shock factor 1 (Hsf1) is a central actor in Protein Quality Control (PQC) and protein
51 homeostasis (proteostasis) in eukaryotes, in both stressed and unstressed cell, and in pathological
52 situations [7]. Notably, Hsf1 is a direct modulator of tumorigenesis and becomes essential, as it is in
53 budding yeast [8], to support growth of malignant cells [9]. Hsf1 prevents protein aggregation and
54 proteome imbalance by driving the expression of a small regulon including genes encoding essential
55 chaperones (Hsp70/Hsp90), nuclear/cytoplasmic aggregases, and proteasome components [8,10,11].
56 Interestingly, studies in budding yeast reveal that the Ribosome Quality Control complex (RQC),
57 conserved from yeast to human [12], increases Hsf1 activity under conditions of translation stress.
58 However, many essential aspects of Hsf1 regulation remain to be elucidated, in particular whether its
59 transcriptional activity is linked to ribosome biogenesis itself. Recently, a conserved PQC mechanism
60 referred to as Excess Ribosomal Protein Quality Control (ERISQ) was described that specifically
61 recognizes unassembled RPs in the nucleus and targets them for proteasome degradation [13,14],
62 thus illuminating observations made 40 years ago showing that excess RPs are rapidly degraded
63 [15,16]. Sung and colleagues showed that the ubiquitin ligase Tom1 plays an important role in ESRIQ

64 by preventing the accumulation of detergent-insoluble RPs. The potential role of Hsf1 in ERISQ has
65 not yet been explored.

66 Given the tremendous investment of cellular resources involved in ribosome production [1]
67 and the fact that a decrease of ribosome abundance protects cells against proteotoxic stress [17,18] it
68 might be expected that cells have evolved mechanisms to rapidly decrease RP gene transcription in
69 the face of defects in ribosome assembly, in order to both save energy and reestablish cellular
70 proteostasis. In *S. cerevisiae*, RP gene transcription is known to be tightly regulated according to
71 growth conditions through the stress-sensitive transcription factor (TF) Ifh1. Thus, Ifh1 is rapidly
72 released from RP promoters only minutes following inhibition of the conserved eukaryotic growth
73 regulator Target Of Rapamycin Complex 1 (TORC1) kinase [19]. Although it has been shown that Ifh1
74 promoter binding is coordinated with RNA polymerase I (RNAPI) activity upon prolonged TORC1
75 inhibition to help balance RP and rRNA production [20,21], how Ifh1 is removed from RP gene
76 promoters to immediately down-regulate their expression following stress remains a mystery.
77 Furthermore, possible links between RP gene expression, ribosomal assembly and the protein
78 homeostasis transcription program driven by Hsf1 remain important open questions.

79 In this study we uncover a novel regulatory pathway, hereafter referred to as the Ribosomal
80 Assembly Stress Response (RASTR), that allows rapid and simultaneous up-regulation of protein
81 homeostasis genes and down-regulation of RP genes following disruption of various steps in ribosome
82 biogenesis (rRNA production, processing or RP assembly). We show that RASTR is highly specific to
83 the RP and Hsf1 regulons, with little or no effect on a much larger group of genes implicated in the
84 Environmental Stress Response (ESR). Importantly, RASTR requires neo-synthesis of RPs following
85 stress and is linked to the accumulation of RP aggregates, which we propose lead to Hsf1 activation,
86 through chaperone competition, and to the sequestration of Ifh1 in an insoluble nucleolar fraction.
87 Notably, we show that protein synthesis inhibition via cycloheximide treatment leads to a
88 transcriptional response opposite to that of RASTR, supporting a model in which unstressed cells
89 constantly monitor nuclear levels of unassembled RPs and use this information to balance expression
90 of Hsf1 target genes with those encoding RPs. Finally, we demonstrate that RASTR is the initial
91 transcriptional response to inactivation of TORC1 kinase, supporting a key role for this regulatory

pathway in the activation of a protein homeostasis transcriptional program that allows cells to cope with the proteotoxic consequences of disruptions to ribosome biogenesis.

Results

Topoisomerase depletion triggers a rapid repression of RP genes and activation of proteostasis genes

In an effort to better understand the role of the two major eukaryotic DNA topoisomerases in protein-coding gene transcription, we generated yeast strains in which Top1, Top2, or both of these enzymes are rapidly degraded by the auxin-induced degron (AID) method ([22] and confirmed by Western blotting that significant depletion of either protein was obtained between 10 and 20 minutes following auxin addition to the medium, and that Top2 depletion, as expected, prevents cell growth (**Figure 1-figure supplement 1A, B**). We then performed ChIP-seq analysis of RNA polymerase II (RNAPII) in the Top1-AID, Top2-AID and Top1/2-AID strains at 20 and 60 minutes following auxin addition (**Figure 1A-C, Supplementary File 1**). As expected [23,24], the absence of Top2 had little or no effect on RNAPII distribution (**Figure 1B**). However, Top1 depletion triggered a rapid response at two specific groups of genes: up-regulation of Hsf1 target genes and down-regulation of ribosomal protein (RP) genes (**Figure 1A, D; Figure 1-figure supplement 1C, D**). Remarkably, this response was transient, as both groups of genes returned to normal levels (i.e. before auxin addition) by 60 minutes. This re-equilibration was dependent upon Top2 since it failed to occur in the Top1/2-AID strain, where prolonged auxin treatment led to significant dysregulation of many other RNAPII-transcribed genes (**Figure 1C**).

Since up-regulation of proteostasis-related genes and down-regulation of RP genes are characteristic of many different stress responses, we decided to quantify the effect of Top1 depletion on transcription all gene groups that have been classified as part of the general “Environmental Stress Response” (ESR; [25]), which include an additional group of stress-induced genes regulated by the Msn2/4 TFs and a large suite of genes involved in ribosome biogenesis (RiBi genes). This analysis shows clearly that Top1 depletion, as well as depletion of both Top1 and Top2 (at the early 20-minute

time point), triggers a highly specific stress response linked to RP genes and Hsf1 target genes (**Figure 1A-C**). Such a targeted response is unlikely to result from a global topological effect on RNAPII recruitment but would instead appear to be the consequence of the activation of a specific signaling pathway that is more restricted in nature than the ESR.

To explore the target(s) of this hypothetical signaling pathway at RP genes we monitored by qPCR ChIP the promoter association of three TFs (Rap1, Fhl1 and Ifh1) that operate at the majority (>90%) of these 138 genes [26]. Interestingly, we found that the activator Ifh1 is rapidly released from RP gene promoters after topoisomerases depletion (**Figure 1E**) whereas Rap1 and Fhl1, which bind directly to RP promoter DNA, are not affected (**Figure 1-figure supplement 1E-F**). To confirm that Hsf1 is indeed required for up-regulation of genes following Top1 depletion we used the anchor-away technique [27] to rapidly remove Hsf1 from the nucleus (30 minutes treatment with rapamycin; [8]) before initiating Top1-AID degradation by auxin addition (**Figure 1F**). Efficient nuclear depletion of Hsf1 was confirmed by the inability of the Hsf1-FRB, Top1-AID strain to form colonies in the presence of rapamycin (**Figure 1-figure supplement 1G**). Note that the strain used in this and all other anchor-away experiments contains the *TOR1-1* mutation and is thus resistant to the normal physiological consequences of rapamycin treatment, which inactivates the growth-promoting TORC1 kinase [28,29]. This experiment revealed that Hsf1 nuclear depletion completely abolishes activation of stress genes following Top1 depletion without affecting down-regulation of RP genes (**Figure 1G**). Therefore, activation of stress-induced genes following Top1 depletion is completely Hsf1-dependent, whereas repression of RP genes is independent of Hsf1 or the induction of its target genes. We would also note that the stress pathway induced by Top1 depletion is unusually restricted in comparison to many other stress responses that are often grouped together as the Environmental Stress Response (ESR; [25]), since *Msn2/4* target genes are not induced and *RiBi* genes are not down-regulated (**Figure 1A, G**).

Top1 depletion arrests ribosome biogenesis and activates a ribosomal assembly stress response

Although it may seem surprising that depletion of topoisomerases can induce a Hsf1-dependent stress response, formation of distinct nuclear foci by the Btn2 aggregase and perinuclear accumulation of the proteasome subunit Pre6 following Top1/2 degradation (**Figure 2-figure**

supplement 1A, B) both point to the induction of proteotoxic stress in the nucleus [30]. Top1 was initially identified through a mutation (*mak1*) defective in large ribosomal subunit production [31] and was later shown to be required for proper rRNA synthesis [23,32,33]. Consistent with these findings, we observed a strong reduction of pre-rRNA synthesis as shown by decreased [³H]-adenine pulse-labelling of the RNAPI-transcribed 35S pre-rRNA, and two co-transcriptionally cleaved products, 27S and 20S pre-rRNAs, as early as 10 minutes after initiation of Top1 (or Top1 and Top2) depletion by addition of auxin to the medium (**Figure 2-figure supplement 1C**). This decreased rRNA synthesis is accompanied by an elongation defect, as shown by the accumulation of truncated pre-rRNAs that were initially described by the Tollervey laboratory ([32]; **Figure 2A**). Further downstream, the rapid defect in rRNA production caused by inhibition of RNAPI elongation leads to unbalanced production of 40S and 60S ribosomal subunits, with a marked deficiency of the large (60S) subunit relative to the small (40S) subunit (**Figure 2B**). This would be expected to create a disequilibrium between RP and rRNA production, and more specifically an excess of unassembled RPs. Consistent with this, we detect accumulation of both and large and small subunit proteins (Rpl3 and Rps8, respectively) in trailing fractions of polysome gradients (**Figure 2C**). These observations strongly suggest that RPs fail to be incorporated normally into ribosomes immediately following topoisomerase degradation. In addition, this sedimentation profile may also reflect the presence of disassembling or incompletely assembled pre-60S particles. RPs are known to be prone to aggregation [2-5] and recent reports show that newly-synthetized, unassembled RPs accumulate in aggregates in response to ribosome assembly stress [13,14]. Significantly, we also observed accumulation of RPs in an insoluble fraction following topoisomerase degradation (**Figure 2D**).

The observations described above led us to hypothesize that the transcriptional response to Top1 degradation is a consequence of defective ribosome assembly, perhaps driven by the proteotoxic stress caused by the accumulation of unassembled RPs. To challenge this idea, we measured the transcriptional response to three different perturbations to ribosome biogenesis: depletion of two essential ribosome assembly factors (Utp8 and Utp13) and treatment of cells with diazaborine. Utp8p is a member of the t-UTP subcomplex of 90S pre-ribosomes and its depletion inhibits rDNA transcription, leading to a reduction of the primary 35S pre-rRNA transcript and

subsequent processing intermediates [34]. In contrast, depletion of Utp13 (a member of the UTP-B subcomplex) interferes with downstream processing and synthesis of 40S subunits and causes decreased 18S rRNA levels without affecting the levels of the 25S or 5.8S rRNAs [34]. Diazaborine, an inhibitor of the essential Drg1 AAA-ATPase, rapidly blocks mid-late steps of 60S subunit maturation [35]. Remarkably, all of these treatments triggered a similar transcriptional response to that which occurs following Top1 depletion, namely a specific down-regulation of RP genes and up-regulation of Hsf1 target genes (**Figure 2E-G; Supplementary File 2**), which we refer to as the “Ribosome Assembly STress Response” (RASTR).

Hsf1 activity is stimulated by many different types of cellular stress, including stalled ribosomes. A pioneering study reported that a set of proteins termed the Ribosome Quality Control Complex (RQC) binds to 60S ribosomal subunits containing stalled polypeptides and leads to their degradation. In the process, the RQC triggers a specific stress signal that leads to Hsf1 target gene activation [12]. Thus, cells lacking a component of the RQC, the Tae2 protein, fail to activate Hsf1 following translational stress. To ask if RASTR might be related to the RQC, we induced Top1/2 degradation in *tae2-Δ* cells. We found that activation of two Hsf1 target genes (*SSA1* and *HSP42*) and down-regulation of two RP genes (*RPL30* and *RPL39*) was unaffected by deletion of *TAE2* (**Figure 2-figure supplement 1D**) and conclude that RQC does not play a role in RASTR. These results highlight that cells have developed distinct mechanisms to adapt the Hsf1 transcriptional program to defects in both ribosome activity and ribosome assembly.

Ifh1 sequestration in an insoluble nuclear fraction during RASTR is driven by RP accumulation

Although many studies would support the notion that Hsf1 activation during RASTR occurs through sequestration of its inhibitory partner Hsp70 by RP aggregates [36-38], it is less clear how ribosome assembly stress could trigger release of Ifh1 from RP gene promoters. We reported previously that the association of Ifh1 with RP gene promoters in growing cells is rapidly disrupted (within 5 min) following inhibition of the growth-promoting TORC1 kinase by addition of rapamycin to the medium [19]. More recently [20], we found that stable release of Ifh1 from RP gene promoters (measured 20 min after rapamycin addition) requires its C-terminal domain together with a complex of proteins containing casein kinase 2 (CK2) and two RiBi factors, Utp22 and Rrp7, with which Ifh1

interacts to form the CUR1 complex [21]. Thus, in *ifh1-ΔC* cells the truncated protein is rapidly released but later returns to RP gene promoters following TORC1 inhibition. This led us to propose two distinct mechanisms controlling the promoter release of Ifh1 following stress: one operating at a short timescale (< 5 min) and the other on a long timescale (~20 min). Interestingly, *ifh1-ΔC* promoter release is stable following Top1 depletion, suggesting that an unknown mechanism regulates Ifh1 during RASTR (**Figure 3A**).

The fact that RP gene repression and Hsf1 target gene activation occur with identical kinetics following RASTR activation (**Figure 3B**), and that Ifh1 concentrates in nuclear foci rapidly after topoisomerase depletion (**Figure 3C**), suggests that Ifh1 could be sensitive to the accumulation of unassembled RPs in the nucleus, as is presumably the case for Hsf1. Several lines of evidence are consistent with this hypothesis. To begin with, in cells lacking Tom1, an E3 ligase required for degradation of unassembled RPs [13,14], but not in *TOM1* cells, Ifh1 accumulates in prominent nuclear foci even in the absence of stress (**Figure 3D**). This suggests that Ifh1 aggregates in cells that are unable to efficiently degrade excess RPs, even under optimal growth conditions. Consistent with this, the published mass spectrometry data of insoluble fractions from cells either treated with the proteasome inhibitor bortezomib or lacking Tom1 clearly identified Ifh1, together with RPs, RiBi proteins and two Hsp70 proteins, Ssa1 and Ssa2, inhibitory partners of Hsf1 (**Figure 3-figure supplement 1A**). These data indicate that Ifh1 could be trapped in an insoluble cellular fraction in the absence of Tom1 and thus decrease the pool of Ifh1 able to bind with RP gene promoters. To test this possibility, we combined deletion of *TOM1* with a mutant allele of *IFH1* (*ifh1-AA*) that weakens its interaction with RP gene promoters. Remarkably, *tom1-Δ* is synthetically lethal with *ifh1-AA* (**Figure 3E**) supporting the notion that RP aggregation could directly impact on Ifh1 promoter binding. Lastly, to exclude the possibility that the genetic interaction between *TOM1* and the mutated allele of *IFH1* could be linked to the growth defect of this mutation, we examined another mutated allele of *IFH1* (*ifh1-6*) that triggers a similar growth defect (**Figure 3E**). Importantly, we showed in a previous study that this *ifh1-6* mutant protein remains bound at high levels to RP genes promoter even under stress conditions [20]. Remarkably, *tom1-Δ* is not synthetically lethal with *ifh1-6* (**Figure 3E**), supporting the

notion that genetic interaction with *lfh1-AA* is directly linked to the ability of Ifh1 to bind RP gene promoters.

To assess directly whether Ifh1 is sequestered in aggregates during RASTR, we analyzed by mass spectrometry the insoluble fraction following topoisomerase depletion. As previously reported for *tom1-Δ* cells [13], the insoluble fraction is enriched in chaperones and RPs (**Figure 3F, G**). We also noted a strong increase in RiBi factors, primarily those implicated in biogenesis of the large ribosomal subunit (**Figure 3G**). Importantly, Ifh1 was never detected in an insoluble fraction in the absence of stress but was invariably detected in these fractions following topoisomerase depletion (**Supplementary File 3**). This rapid sequestration of Ifh1 may be sufficient to explain the observed down-regulation of RP genes during RASTR.

Neo-synthetized RPs are required for RASTR activation

Given their fast turnover rate, nuclear accumulation in the absence of ribosome assembly and propensity to aggregate, unassembled RPs could be ideally positioned to rapidly signal ribosome biogenesis defects [13,39]. To evaluate the importance of newly synthetized RPs in RASTR, we blocked their production by cytoplasmic anchoring of Ifh1 before topoisomerase depletion (**Figure 4A**). It is important to note that Ifh1 binding is highly specific to RP genes [26] and that the transcriptional effect of its nuclear depletion is restricted to RP genes and a very small number of additional targets (**Supplementary File 4**). Although Ifh1 depletion by anchor-away may not be complete (the strain still grows on plates containing rapamycin, albeit slowly, even though Ifh1 is essential for growth; **Figure 4-figure supplement 1A**), it nonetheless leads to a significant and highly specific decrease in RP gene transcription as measured by RNAPII ChIP-seq (**Figure 4B; Supplementary File 4**). Interestingly, Ifh1 depletion also leads to aberrant rRNA processing (**Figure 4C**) as would expected in conditions where RP levels become limiting [40]. Remarkably, we noted that 60 min of Ifh1 anchoring alone, in the absence of topoisomerase depletion, also caused a significant down-regulation of Hsf1 target genes (**Figure 4D; Supplementary File 4**) even though Ifh1 is absent from the promoters of these genes (**Figure 4-figure supplement 1B**), suggesting that the Hsf1 transcriptional program is continuously influenced by RP production. Consistent with this idea, we found that up-regulation of Hsf1 target genes was either abolished or strongly reduced (**Figure 4E, F, G**;

Supplementary File S4) when Top1 or Top1 and Top2 were degraded following nuclear depletion of Ifh1, indicating that RP production is required for Hsf1 target gene activation during RASTR.

Cells balance RP production and Hsf1 activity even in the absence of stress

As an alternative approach to test the requirement for *de novo* RP synthesis to initiate RASTR we used cycloheximide treatment, which blocks all translational elongation, thus leading to rapid depletion of the nuclear pools of RPs (**Figure 5A**; [15,16,40,41]). As reported by others [40], we confirmed that cycloheximide alone also triggers a rapid arrest of rRNA processing (**Figure 5B**). Quite strikingly, we observed a transcriptional response to cycloheximide treatment exactly opposite to that induced by RASTR, namely Hsf1 target gene down-regulation and RP gene up-regulation (**Figure 5C**; **Supplementary File 5**). This finding suggests that even in unstressed cells RP production may contribute to a basal level of Hsf1 activation while at the same time limiting Ifh1 activity at RP gene promoters.

Significantly, treatment of cells undergoing Top1 or Top1/2 depletion with cycloheximide (auxin + CHX) completely abolished both RP gene repression and activation of Hsf1 target genes (**Figure 5D, E**; **Supplementary File 5**). Indeed, Hsf1 target gene activation under these conditions is lower than in untreated cells and not significantly different than that seen in cells treated with cycloheximide alone (**Figure 5-figure supplement 1A**). These findings clearly demonstrate that RASTR is dependent upon *de novo* protein synthesis. Importantly, it was recently reported that cycloheximide treatment efficiently prevents aggregation of newly synthesized RPs following proteasome inhibition [13]. Perhaps as a direct consequence of this, we found that CHX treatment also leads to strong reduction of Ifh1-eGFP nuclear foci that are observed in cells lacking the ubiquitin ligase Tom1, which is specifically required for efficient degradation of unassembled RPs ([13,14]; **Figure 5-figure supplement 1B**). Furthermore, Ifh1 dis-aggregation following cycloheximide exposure is associated with increased Ifh1 binding at a RP gene promoter, which becomes significant in *tom1-Δ* cells (**Figure 5-figure supplement 1C**). Similarly, cycloheximide treatment also prevents the release of Ifh1 from RP gene promoters in response to the activation of RASTR by topoisomerase depletion (**Figure 5-figure supplement 1D**). Considered as a whole, these data suggest that both RP and Ifh1 subnuclear structures (aggregates) are dynamic, promoted by *de novo* RP production upon RASTR

initiation, and capable of influencing Ifh1 promoter binding. Consistent with this view, we observed a large increase in cells that accumulate RP (Rpl25) or Ifh1 nuclear aggregates during RASTR that is abolished in the presence of cycloheximide (**Figure 5F, G; Figure 5-figure supplement 1E, F**)

Taken together with the strong reduction of Hsf1 target gene activation following Ifh1 cytoplasmic anchoring, both in the presence and absence of topoisomerase degradation, our observations on the effect of cycloheximide highlight the interwoven nature of RP and Hsf1 target gene regulons and support the notion that unassembled, aggregated RPs constitute the primary RASTR-induced signal capable of regulating both Ifh1 and Hsf1 activities, albeit in an opposite direction. More generally, these data indicate that newly synthesized RPs, in both stressed and unstressed cells, operate as a central hub in coordinating the expression of RP genes themselves with the Hsf1-dependent activation of chaperone and proteasome genes.

RASTR is the first transcriptional response to environmental stress

We next turned our attention to the potential involvement of RASTR during more general stress responses that might also rapidly affect ribosome assembly. In an initial set of experiments, we inactivated the conserved growth-promoting TORC1 kinase by treatment of cells with rapamycin, which is known to mimic a major part of the environmental stress response, including osmotic and redox stress, as well as carbon, nitrogen, phosphate or amino acid starvation [29]. As reported previously, rapamycin triggers a rapid arrest of rRNA processing (**Figure 6A**) and a decrease of RP and RiBi gene expression (**Figure 6B, C; Supplementary File 6**). Interestingly, we noted that Hsf1 target genes are transiently up- and down-regulated at 5 and 20 minutes, respectively, following rapamycin addition (**Figure 6B, C; Supplementary File 6**), suggesting that RASTR is activated at the early time point but shortly thereafter turned off. Consistent with this view, it has been reported that RP production ceases around 15 minutes after rapamycin treatment [40], which we suggest would turn off the signal for RASTR, thus explaining the down-regulation of Hsf1 target genes observed at 20 minutes.

To explore this hypothesis further, we took advantage of our observation that cycloheximide treatment prevents RASTR activation by either Top1 or Top1/2 degradation (**Figure 5**) and treated

cells with cycloheximide 5 minutes before rapamycin addition of either 5 or 20 minutes (**Figure 6D**, see schematics of experimental protocols below the respective panels). Remarkably, this specifically prevented RP gene repression and Hsf1 target gene activation at 5 minutes following rapamycin addition, whereas at the longer time point (20 minutes) RP genes and Hsf1 were regulated independently of cycloheximide (**Figure 6D, E; Supplementary File 6**). Consistent with the early block in RP gene down-regulation being due to a failure to initiate RASTR immediately following rapamycin addition, we showed that cycloheximide pre-treatment prevents release of Ifh1 from RP gene promoters at 5 minutes, but not at 20 minutes following rapamycin treatment (**Figure 6F**).

The effects of rapamycin treatment described above are fully consistent with our previous report demonstrating that regulation of RP gene transcription following TORC1 inactivation by rapamycin operates through two distinct mechanisms at short and long timescales, with the latter dependent on RNAPI activity and the CURI complex [20]. The short timescale mechanism described here, which is dependent upon continued protein synthesis and presumably mediated by RASTR, allows cells to rapidly arrest RP production and avoid or minimize proteotoxic stress induced by arrested ribosome assembly. The second mechanism permits the resumption of RP production only when rRNA synthesis also resumes [20]. These two mechanisms could be particularly useful to rapidly adapt ribosome production to new growth conditions.

To explore the possible generality of rapid RASTR-mediated shut-down of RP gene transcription in response to stress, we measured the transcriptional response to heat shock, which is known to transiently down-regulate both RP gene and rRNA transcription [25,42]. As expected, we observed strong down-regulation of RP genes and up-regulation of Hsf1 target genes only 5 minutes following a shift in temperature to 40°C (**Figure 7A-C**, left panels) that was also accompanied by strong up-regulation of Msn2 target genes and down-regulation of RiBi genes (**Figure 7A**, left panel). The heat shock transcriptional response is thus much broader than that to ribosome assembly stress, despite their common effects on RP and Hsf1 target gene expression. Remarkably, though, we found that cycloheximide pre-treatment prevents the strong and immediate repression of RP genes following heat shock (**Figure 7A, B; right panels; Supplementary File 6**), consistent again with the idea that this facet of the heat shock response is identical to that which occurs during RASTR. Importantly

though, Hsf1 target genes are still activated following heat shock in the presence of cycloheximide (Figure 7A, C; right panels), presumably because the unfolding of thermo-labile proteins induced by heat shock is alone sufficient to activate Hsf1 even in the absence of continuing RP synthesis. Nevertheless, the striking requirement for *de novo* protein synthesis for RP gene down-regulation following heat shock strongly suggests that RASTR plays an integral role in this component of the heat shock response and thus may constitute the earliest transcriptional response, at the level of RNAPII, to a wide variety of stress conditions.

Discussion

In this study we demonstrate the existence of a regulatory mechanism, which we refer to as the ribosome assembly stress response, or RASTR, that allows yeast cells to specifically coordinate the activity of two TFs, Hsf1 and Ifh1, with the functional state of ribosome assembly. Our data and several previous reports suggest that rapid ribosome biogenesis is a potentially proteotoxic process, in large part due to accumulation of unassembled RPs, whose production needs to be carefully coordinated at the transcriptional level, at least in yeast, together with that of chaperones and proteasome components (Figure 8). In this perspective, RASTR may play an essential role in minimizing the proteostasis burden imposed by high ribosome production rates, particularly under fluctuating environmental conditions.

Our data indicate that disequilibrium at any step-in ribosome biogenesis (rRNA transcription, early or late rRNA processing or assembly) will lead to RASTR activation until the pool of unassembled RPs decreases. Consequently, proteasome inhibition [42], dNTP depletion [43], DNA damage [44], nutrient and thermal stress [45,46], all of which are known to alter rRNA transcription or processing, or ribosome assembly (reviewed in [6]), are likely to activate RASTR, as do the genetic perturbations at different step of ribosome assembly described here. Taken together with previous reports, our data thus point to a critical role for RASTR in the transcriptional networks regulating both growth and protein homeostasis.

It is important to note that RPs are among the most abundant ubiquitinated proteins that accumulate in the nucleus of proteasome-deficient *S. cerevisiae* and human cells [13,14,41,47], suggesting that the synthesis of RPs and their assembly into ribosomes must be tightly coordinated with the cell's proteostasis capacity. Consistent with this view, we show here that induction of ribosome assembly stress is correlated with the rapid accumulation of RPs in a detergent-insoluble fraction and that blocking *de novo* RP production, either by anchoring away Ifh1 or treating cells with cycloheximide, diminishes or abolishes a key transcriptional consequence of RASTR, namely up-regulation of Hsf1 target genes. Our observations thus strongly suggest that RP aggregates are an important activating signal for RASTR. Nevertheless, we and others [13] detect a large number of additional proteins that accumulate in an insoluble fraction upon ribosome assembly stress, including many RiBi proteins (e.g. numerous rRNA helicases and processing factors), the RP gene activator Ifh1, and chaperones. At present we do not know the precise molecular nature of these aggregates, which presumably accumulate in the nucleolar space, or even whether they represent a common structure. In any event, our data suggest that RP- and Ifh1-containing aggregates are highly dynamic since the promoter release of Ifh1 and activation of Hsf1 following Top1 degradation are rapidly reversed by Top2 compensation (**Figure 1**) and Ifh1 aggregates that appear in *tom1-Δ* cells quickly diminish following cycloheximide treatment (**Figure 5-figure supplement 1A**). We imagine that this provides a strong selective advantage by allowing cells to rapidly recover from a transient disruption of ribosome biogenesis.

Accumulation of proteins in insoluble fractions or aggregates underlies numerous diseases, as well as aging [48,49]. However, certain protein aggregates appear to be dynamic structures that contribute to cellular fitness by protecting the cell during stress [50-54]. For example, stress granules and P-bodies, two of the most intensively studied insoluble macromolecular aggregates, have emerged as important cytoplasmic regulators of gene expression by controlling the processing, sequestering and/or degradation of specific RNA transcripts [55,56]. Interestingly, it has recently been reported that nucleolar proteins can form sub-compartmental structures by promoting liquid-liquid phase separation [57,58]. Although further work will be required to characterize the composition, assembly and function of these nucleolar membrane-less structures, they are attractive

395 candidates for regulatory hubs that could act by sensing ribosome biogenesis stress and controlling
396 adaptive responses. With respect to the present study, we imagine that liquid phase-separated
397 structures in the nucleolus could be directly involved in sequestration of Ifh1 during RASTR, as well as
398 the titration of Hsp70 that we propose leads to Hsf1 activation. A challenge for future studies will be
399 to characterize the physical properties of these postulated structures and their relevance to the
400 transcriptional outputs that we measure here.

401 We showed previously [20] that in strains where RNAPI is constitutively active [59] Ifh1 is
402 released from RP gene promoters shortly after TORC1 inhibition by rapamycin treatment (~5
403 minutes) but returns only 15 minutes later. This promoter re-binding does not occur in wild-type cells
404 due to the action of two RiBi proteins (Utp22 and Rrp7) that can sequester Ifh1 in the CURI (Casein
405 Kinase 2/Utp22/Rrp7/Ifh1) complex [20,21] allowing to re-align RP gene expression with RNAPI
406 activity. These findings revealed that *S. cerevisiae* has developed temporally distinct mechanisms to
407 regulate RP gene expression. One of the keys finding in the present study is to confirm the existence
408 of a two-step process in RP gene regulation and to link the first step to control of the Hsf1 regulon.
409 We propose that this short timescale mechanism results from a rapid rise in unassembled RPs that
410 occurs immediately following TORC1 inhibition, or other stresses that disrupt ribosome assembly,
411 such as depletion of Top1 or RiBi factors.

412 Following ribosome assembly stress, we imagine that the rapid induction of Hsf1 target
413 genes, in combination with the arrest of RP gene transcription, contributes to the eventual clearing of
414 proteotoxic unassembled RPs from the nucleus, thereby removing the signal that promotes RASTR
415 and leads to Ifh1 promoter release and Hsf1 activation. Accordingly, RP production is abolished by 20
416 minutes following TORC1 inhibition [40], suggesting that RASTR becomes inoperant, thus explaining
417 the downregulation of Hsf1 genes (**Figure 6B**) and the switch to a secondary regulatory mechanism,
418 involving sequestration of Ifh1 in the CURI complex, to align RP expression with rRNA production [20].
419 Consistent with this view, the short time scale mechanism of RP gene down-regulation is abolished by
420 attenuating proteotoxicity through translation inhibition (cycloheximide treatment) whereas the long
421 time scale process is insensitive to translation arrest but can be prevented by expression of a
422 constitutively active RNAPI [20,59]. These two independent mechanisms adapt RP gene expression to

both rRNA production and ribosome assembly, thus minimizing the accumulation of unassembled RPs.

As alluded to above, ribosome assembly stress in higher eukaryotes has been studied extensively in the context of ribosomopathies, diseases often associated with RP gene haplo-insufficiencies, RP gene point mutations or mutations in RiBi factors. One hypothesis put forward to explain these observations is that unassembled RPs trigger a feedback mechanism that decreases transcription of ribosome biogenesis genes by inhibiting c-Myc function and arrests cell growth through p53 activation [60,61]. It has also been recently reported that the rRNA helicase DDX21 binds to and activates RP gene promoters in a manner that may be sensitive to the status of ribosome biogenesis [62]. Taken together, these findings suggest that unassembled RPs could mediate an ancestral process to regulate ribosome biogenesis conserved from prokaryotes [63] to eukaryotes. Transcriptome analysis immediately following ribosome assembly stress in mammalian cells will be required to understand the interplay between these different mechanisms and may also uncover novel pathways.

Our work also provides insights into the connection between ribosome assembly and Hsf1 that was first revealed in a report from the Churchman lab that appeared as our work was being prepared for publication (<http://dx.doi.org/10.1101/458810>). Hsf1 is a key sensor of proteotoxic stress in all eukaryotes that controls a common set of chaperones conserved from yeast to human. One protective function reported for Hsf1 is its ability to reduce protein aggregate formation leading to neurodegenerative diseases [64]. On the other hand, Hsf1 also exerts a pro-oncogenic function through its ability to promote proteostasis in rapidly growing tumor cells [65,66]. Despite its central function, a holistic understanding of the regulatory mechanisms that govern Hsf1 activity still missing. Our work and that of Tye et al. (<http://dx.doi.org/10.1101/458810>) demonstrates that Hsf1 activity is tightly linked to ribosome biogenesis in yeast, in a manner independent of the previously described RQC mechanism that contributes to the dissociation of aberrant nascent polypeptides from the ribosome [12]. These two mechanisms highlight the central importance of ribosome assembly and activity in regulation of cellular protein homeostasis through Hsf1. Although it is currently unknown if RASTR is conserved in metazoans, we note that RPs are also subjected to a high turnover rate

451 compared to other nuclear components in mammalian cells and that proteasome or ribosome
452 assembly inhibition trigger a rapid accumulation of RPs in the nucleus, whereas arrest of translation
453 has an opposite effect [13,41]. Importantly, it was reported that cycloheximide treatment also
454 abolishes Hsf1 activity in mammalian cell by an unknown mechanism [9]. We propose that a dynamic
455 balance between unassembled and assembled RPs could be sensed by Hsf1 to constantly adjust
456 protein homeostasis transcription programs in eukaryotes with translational flux, proteolysis and the
457 rate of ribosome assembly (**Figure 8**), since disruption or hyperactivation of any of these processes
458 will rapidly change nuclear levels of free RPs. Given the growing body of evidence linking Hsf1 activity
459 to numerous diseases associated with proteotoxic stress, but also rapid cell growth in cancer, it will
460 be of great interest to challenge this model in the future.

461

Materials and Methods

Key Resources Table

Reagent type	Designation	Source or reference	Identifiers	Additional information
chemical compound, drug	Cycloheximide	Sigma	C7698	Materials & Methods subsection: Yeast strains and growth
chemical compound, drug	Rapamycin	Sigma	R8781	Materials & Methods subsection: Yeast strains and growth
chemical compound, drug	Auxin	Sigma	1288G	Materials & Methods subsection: Yeast strains and growth
chemical compound, drug	Diazaborine	provided by H. Bergler. Zisser et al., 2018	PMID: 29294095	Materials & Methods subsection: Yeast strains and growth
commercial assay or kit	TruSeq ChIP Sample Preparation Kit	Illumina	IP-202-9001DOC	
antibody, rabbit polyclonal	Anti-RNA polymerase II CTD repeat YSPTSPS (phospho S5)	Abcam	ab5131	Rabbit polyclonal; (1ug per ChIP (50ml OD=0.5))
antibody, rabbit polyclonal	anti-Rap1	N/A Schawalter et al., 2004 (PMID:15616569)	RRID AB_2801428	Rabbit polyclonal; (5ul per ChIP (50ml OD=0.5))
antibody	anti-Rpl3	provided by J. Warner and S. Buhl. Vilardell & Warner, 1997.	PMID: 9121443	Results, Figure 5. Mouse monoclonal; 1:10 000
antibody	anti-Rpl6	provided by O. Gadal		Rabbit polyclonal; 1:10 000
antibody	anti-Rps8	provided by G. Dieci		Rabbit polyclonal; 1:10 000
antibody, rabbit polyclonal	antibody Ifh1	N/A (Knight et al., 2015) PMID: 25085421	AB_2801429	Rabbit polyclonal (2ul per ChIP (50ml OD=0.5))
antibody, rabbit polyclonal	antibody Fhl1	N/A (Knight et al., 2015) PMID: 25085421	AB_2801431	Rabbit polyclonal (2ul per ChIP (50ml OD=0.5))
Strain, strain background	<i>Saccharomyces cerevisiae</i> , W303	W303: <i>MATa/MATa leu2-3,112 trp1-1 can1-100 ura3-1 ade2-1 his3-11,15</i>	Thomas & Rothstein, 1989. PMID: 2645056. Experimental procedures, Strains. Table 1.	See Supplementary File 7
other	Primary sequence files	GEO	accession number GSE125226	Materials & Methods subsection: Plasmid construction
recombinant DNA reagent	pFA6a-link-GFPEnvy-SpHis5 (plasmid)	Addgene	RRID: Addgene_60782	Materials & Methods subsection: Plasmid construction
recombinant DNA reagent	RPL25-envyGFP-plasmid	this paper	Plasmid #1037	Materials & Methods subsection: Plasmid construction
recombinant DNA reagent	pRS315-RPL25-eGFP	Gadal et al., 2001 PMID: 11313466		Materials & Methods subsection: Plasmid constructions

ChIP-Seq

Cultures of 50 mL in YPAD were collected at OD₆₀₀ 0.4 - 0.8 for each condition. The cells were crosslinked with 1% formaldehyde for 5 min at room temperature and quenched by adding 125 mM glycine for 5 min at room temperature. Cells were washed with ice-cold HBS and resuspended in 3.6 mL of ChIP lysis buffer (50 mM HEPES-Na pH 7.5, 140 mM NaCl, 1mM EDTA, 1% NP-40, 0.1% sodium deoxycholate) supplemented with 1mM PMSF and 1x protease inhibitor cocktail (Roche). Samples were aliquoted in Eppendorf tubes and frozen. After thawing, the cells were broken using Zirconia/Silica beads (BioSpec). The lysate was spun at 13,000 rpm for 30 min at 4°C and the pellet was resuspended in 300 µl ChIP lysis buffer + 1mM PMSF and sonicated for 15 min (30 sec ON - 60 sec OFF) in a Bioruptor (Diagenode). The lysate was spun at 7000 rpm for 15 min at 4°C. Antibody (1 µg / 300 µL of lysate, Abcam ab5131) was added to the supernatant and incubated for 1 hr at 4°C. Magnetic beads were washed three times with PBS plus 0.5% BSA and added to the lysates (30 µL of beads/300 µL of lysate). The samples were incubated for 2 hr at 4°C. The beads were washed twice with (50 mM HEPES-Na pH 7.5, 140 mM NaCl, 1mM EDTA, 0.03% SDS), once with AT2 buffer (50 mM HEPES-Na pH 7.5, 1 M NaCl, 1mM EDTA), once with AT3 buffer (20 mM Tris-Cl pH 7.5, 250 mM LiCl, 1mM EDTA, 0.5% NP-40, 0.5% sodium deoxycholate) and twice with TE. The chromatin was eluted from the beads by resuspension in TE + 1% SDS and incubation at 65°C for 10 min. The eluate was transferred to an Eppendorf tube and incubated overnight at 65°C to reverse the crosslinks. The DNA was purified using High Pure PCR Cleanup Micro Kit (Roche). DNA libraries were prepared using TruSeq ChIP Sample Preparation Kit (Illumina) according to manufacturer's instructions. The libraries were sequenced using an Illumina HiSeq 2500 and the reads were mapped to the sacCer3 genome assembly using HTSStation (shift = 150 bp, extension = 50 bp; [67]). To compare depleted versus non-depleted cells, we divided the signal from the +auxin and/or rapamycin and/or cycloheximide samples by the signal from the – auxin and/or rapamycin and/or cycloheximide (vehicle) samples and log2 transformed this value. All data from publicly available databases were mapped using HTS Station (<http://htsstation.epfl.ch>; [67]).

Yeast strains, primer DNAs and cell growth

Strains used in this study are listed in **Supplementary File 7**. For ChIP-qPCR, the primer sequences used are listed in **Supplementary File 8**. Experiments were typically performed with log phase cells harvested between OD₆₀₀ 0.4 and 0.8. Anchor-away of FRB-tagged proteins was induced by the addition of rapamycin (1 mg/ml of 90% ethanol/10% Tween stock solution) to a final concentration of 1 µg/ml [27]. Depletion of AID-tagged protein was induced by the addition of auxin (3-indoloacetic acid) at 500 µM final concentration. Arrest of translation was induced by the addition of cycloheximide to a final concentration of 25 µg/ml. Cells are treated with diazaborine to a final concentration of 50 µg/ml.

Fluorescence microscopy

Cells were grown overnight at 30°C in SC medium (0.67% nitrogen base without amino acids (BD), 2% dextrose supplemented with amino acids mixture (AA mixture; Bio101), adenine, and uracil). Cells were diluted and were harvested when OD₆₀₀ reached 0.4. Cells were spread on slides coated with an SC medium patch containing 2% glucose. Stacked images were recorded (Intelligent Imaging Innovations) at a spinning disc confocal inverted microscope (Leica DMIRE2) using the 100x oil objective and an Evolve EMCCD Camera (Photometrics).

Insoluble fraction purification and mass spectrometry

Isolation of protein aggregates from yeast cells was performed as described previously [68] with slight modifications. 50 OD₆₀₀ units (50 ml) of exponentially growing cells were harvested, and cell pellets were frozen in liquid N₂. The cell pellets were resuspended in 1 ml lysis buffer (20 mM Na-phosphate pH 6.8, 10 mM DTT, 1 mM EDTA, 0.1% Tween, 1 mM PMSF, protease inhibitor cocktail and 100 units/ml zymolyase) and incubated at 30° C for 30 min. Chilled samples were treated by tip sonication (20%, 10 sec, 2x) and centrifuged for 20 min at 600 g at 4°C. Aggregated proteins were pelleted at 16,000 g for 20 min at 4°C. After removing supernatants, insoluble proteins were washed once with Wash I buffer (20 mM Na-phosphate pH 6.8, 500 mM NaCl, 5 mM EDTA, 2% NP-40, 1 mM PMSF, and protease inhibitor cocktail), and centrifuged at 16,000 g for 20 min at 4°C. Insoluble proteins were washed with Wash II buffer (20 mM Na-phosphate pH 6.8, ice-cold), pelleted and sonicated (2x for 10 s) in 40 µl of Wash II buffer. For analysis by SDS-PAGE (4–12% acrylamide) and

subsequent Western blotting, proteins were first boiled in Laemmli buffer. 1x of the total cell lysate and 25x of the insoluble pellet fraction were separated and analyzed by Coomassie Blue staining or immunoblotting. Proteins were identified by shotgun mass spectrometry analysis at the Functional Genomics Center Zurich (ETH, Zurich) following TCA precipitation (20%) and acetone washing, according to posted procedures. Database searches were performed by using the Mascot (SwissProt, all species; SwissProt, yeast) search program, using very stringent settings in Scaffold (1% protein FDR, a minimum of 2 peptides per protein, 0.1% peptide FDR).

Polysome gradients

Yeast cells growing exponentially were treated or not with auxin for 20 min. 50 µg/ml cycloheximide (Sigma) was added directly to the culture medium. Cells were collected by centrifugation, rinsed with buffer K [20 mM Tris-HCl pH 7.4, 50 mM KCl, 10 mM MgCl₂] supplemented with 50 µg/ml cycloheximide and collected again by centrifugation. Dry pellets were resuspended with approximately one volume of ice-cold buffer K supplemented with 1 mM DTT, 1× Complete EDTA-free protease inhibitor cocktail (Roche), 0.1 U/µl RNasin (Promega) and 50 µg/ml cycloheximide. About 250 µl of ice-cold glass beads (Sigma) were added to 500 µl aliquots of the resuspended cells and cells were broken by vigorous shaking, 3 times 2 min, separated by 2 min incubations on ice. Extracts were clarified through 2 successive centrifugations at 13 000 rpm and 4°C for 5 min and quantified by measuring absorbance at 260 nm. About 30 A₂₆₀ units were loaded onto 10% - 50% sucrose gradients in buffer K, and then centrifuged for 150 min at 39,000 rpm and 4°C in an Optima L-100XP Ultracentrifuge (Beckman-Coulter) using a SW41Ti rotor without brake. Following centrifugation, 18 fractions of 500 µl each were collected from the top of the gradients with a Foxy Jr. apparatus (Teledyne ISCO). The absorbance at 254 nm was measured during collection with a UA-6 device (Teledyne ISCO).

Pulse labeling, RNA extraction and Northern hybridization

Metabolic labeling of pre-rRNAs was performed as previously described [69] with the following modifications. Strains were grown in synthetic glucose medium lacking adenine to an OD₆₀₀ of 0.8. Auxin (0.5mM) was next added to the cultures and cells were labeled for 2 min with [2,8-³H]-adenine (NET06300 Perkin Elmer) at 0, 10, 20 and 30 min following the addition of auxin. Cell pellets were

frozen in liquid nitrogen. RNA extractions and Northern hybridizations were performed as previously described [70]. For high molecular weight RNA analysis, 2 µg of total RNA were glyoxal denatured and resolved on a 1.2% agarose gel. Note that Northern hybridization was performed on [2,8-³H]-adenine labeled RNA. The membrane was first exposed to reveal neo-synthetized transcripts, and subsequent Northern hybridization revealed rRNA transcript abundance.

Acknowledgments

We would like to thank Mylène Docquier and the Genomics Platform of iGE3 at the University of Geneva (<https://ige3.genomics.unige.ch/>) for high throughput sequencing services, the Functional Genomics Center Zurich (ETH, Zurich) for mass spectrometry analysis, Prof. Helmut Bergler (Karl-Franzens-Universität, Graz, Austria) for his generous gift of diazaborine, Lyudmil Raykov and the Bioimaging Center at the Faculty of Sciences, University of Geneva (<http://bioimaging.unige.ch/>) for help with confocal microscopy, Nicolas Roggli for expert assistance with data presentation and artwork, Philipp Milkereit and Robbie Loewith for enlightening discussions and all members of the Shore lab for comments and discussions throughout the course of this work. B.A. acknowledges support from a long-term EMBO postdoctoral fellowship in the early phases of this work. M.J.B. was supported in part by an iGE3 Ph.D. student fellowship. D.S. acknowledges funding from the Swiss National Science Foundation (grant number 31003A_170153) and the Republic and Canton of Geneva.

Declaration of interests

The authors declare that they have no competing interests.

Data availability

Read counts for all RNAPII ChIP-seq experiments (integrated counts over the complete open reading frame of all protein-coding genes) are given in Supplementary Tables (**Tables S1-6**). Primary

575 processed sequence files will be made available at Gene Expression Omnibus (GEO accession number
576 GSE125226).
577

References

1. Warner, J.R. The economics of ribosome biosynthesis in yeast. *Trends Biochem Sci* **1999**, *24*, 437-440.
2. David, D.C.; Ollikainen, N.; Trinidad, J.C.; Cary, M.P.; Burlingame, A.L.; Kenyon, C. Widespread protein aggregation as an inherent part of aging in *C. elegans*. *PLoS Biol* **2010**, *8*, e1000450.
3. Pillet, B.; Mitterer, V.; Kressler, D.; Pertschy, B. Hold on to your friends: Dedicated chaperones of ribosomal proteins: Dedicated chaperones mediate the safe transfer of ribosomal proteins to their site of pre-ribosome incorporation. *Bioessays* **2017**, *39*, 1-12.
4. Rand, J.D.; Grant, C.M. The thioredoxin system protects ribosomes against stress-induced aggregation. *Mol Biol Cell* **2006**, *17*, 387-401.
5. Weids, A.J.; Ibstedt, S.; Tamas, M.J.; Grant, C.M. Distinct stress conditions result in aggregation of proteins with similar properties. *Sci Rep* **2016**, *6*, 24554.
6. James, A.; Wang, Y.; Raje, H.; Rosby, R.; DiMario, P. Nucleolar stress with and without p53. *Nucleus* **2014**, *5*, 402-426.
7. Li, J.; Labbadia, J.; Morimoto, R.I. Rethinking HSF1 in Stress, Development, and Organismal Health. *Trends Cell Biol* **2017**, *27*, 895-905.
8. Solis, E.J.; Pandey, J.P.; Zheng, X.; Jin, D.X.; Gupta, P.B.; Airoidi, E.M.; Pincus, D.; Denic, V. Defining the Essential Function of Yeast Hsf1 Reveals a Compact Transcriptional Program for Maintaining Eukaryotic Proteostasis. *Mol Cell* **2016**, *63*, 60-71.
9. Santagata, S.; Mendillo, M.L.; Tang, Y.C.; Subramanian, A.; Perley, C.C.; Roche, S.P.; Wong, B.; Narayan, R.; Kwon, H.; Koeva, M., et al. Tight coordination of protein translation and HSF1 activation supports the anabolic malignant state. *Science* **2013**, *341*, 1238303.
10. Mahat, D.B.; Salamanca, H.H.; Duarte, F.M.; Danko, C.G.; Lis, J.T. Mammalian Heat Shock Response and Mechanisms Underlying Its Genome-wide Transcriptional Regulation. *Mol Cell* **2016**, *62*, 63-78.

- 603 11. Pincus, D.; Anandhakumar, J.; Thiru, P.; Guertin, M.J.; Erkin, A.M.; Gross, D.S. Genetic and
604 epigenetic determinants establish a continuum of Hsf1 occupancy and activity across the
605 yeast genome. *Mol Biol Cell* **2018**, 10.1091/mbc.E18-06-0353, mbcE18060353.
- 606 12. Brandman, O.; Stewart-Ornstein, J.; Wong, D.; Larson, A.; Williams, C.C.; Li, G.W.; Zhou, S.;
607 King, D.; Shen, P.S.; Weibezahn, J., et al. A ribosome-bound quality control complex triggers
608 degradation of nascent peptides and signals translation stress. *Cell* **2012**, 151, 1042-1054.
- 609 13. Sung, M.K.; Porras-Yakushi, T.R.; Reitsma, J.M.; Huber, F.M.; Sweredoski, M.J.; Hoelz, A.;
610 Hess, S.; Deshaies, R.J. A conserved quality-control pathway that mediates degradation of
611 unassembled ribosomal proteins. *Elife* **2016**, 5.
- 612 14. Sung, M.K.; Reitsma, J.M.; Sweredoski, M.J.; Hess, S.; Deshaies, R.J. Ribosomal proteins
613 produced in excess are degraded by the ubiquitin-proteasome system. *Mol Biol Cell* **2016**, 27,
614 2642-2652.
- 615 15. Gorenstein, C.; Warner, J.R. Synthesis and turnover of ribosomal proteins in the absence of
616 60S subunit assembly in *Saccharomyces cerevisiae*. *Mol Gen Genet* **1977**, 157, 327-332.
- 617 16. Warner, J.R. In the absence of ribosomal RNA synthesis, the ribosomal proteins of HeLa cells
618 are synthesized normally and degraded rapidly. *J Mol Biol* **1977**, 115, 315-333.
- 619 17. Guerra-Moreno, A.; Isasa, M.; Bhanu, M.K.; Waterman, D.P.; Eapen, V.V.; Gygi, S.P.; Hanna, J.
620 Proteomic Analysis Identifies Ribosome Reduction as an Effective Proteotoxic Stress
621 Response. *J Biol Chem* **2015**, 290, 29695-29706.
- 622 18. Mills, E.W.; Green, R. Ribosomopathies: There's strength in numbers. *Science* **2017**, 358.
- 623 19. Schawalder, S.B.; Kabani, M.; Howald, I.; Choudhury, U.; Werner, M.; Shore, D. Growth-
624 regulated recruitment of the essential yeast ribosomal protein gene activator Ifh1. *Nature*
625 **2004**, 432, 1058-1061.
- 626 20. Albert, B.; Knight, B.; Merwin, J.; Martin, V.; Ottoz, D.; Gloor, Y.; Bruzzone, M.J.; Rudner, A.;
627 Shore, D. A Molecular Titration System Coordinates Ribosomal Protein Gene Transcription
628 with Ribosomal RNA Synthesis. *Mol Cell* **2016**, 64, 720-733.

- 629 21. Rudra, D.; Mallick, J.; Zhao, Y.; Warner, J.R. Potential interface between ribosomal protein
630 production and pre-rRNA processing. *Mol Cell Biol* **2007**, *27*, 4815-4824.
- 631 22. Nishimura, K.; Fukagawa, T.; Takisawa, H.; Kakimoto, T.; Kanemaki, M. An auxin-based
632 degron system for the rapid depletion of proteins in nonplant cells. *Nat Methods* **2009**, *6*,
633 917-922.
- 634 23. Brill, S.J.; DiNardo, S.; Voelkel-Meiman, K.; Sternglanz, R. Need for DNA topoisomerase
635 activity as a swivel for DNA replication for transcription of ribosomal RNA. *Nature* **1987**, *326*,
636 414-416.
- 637 24. Brill, S.J.; Sternglanz, R. Transcription-dependent DNA supercoiling in yeast DNA
638 topoisomerase mutants. *Cell* **1988**, *54*, 403-411.
- 639 25. Gasch, A.P.; Spellman, P.T.; Kao, C.M.; Carmel-Harel, O.; Eisen, M.B.; Storz, G.; Botstein, D.;
640 Brown, P.O. Genomic expression programs in the response of yeast cells to environmental
641 changes. *Mol Biol Cell* **2000**, *11*, 4241-4257.
- 642 26. Knight, B.; Kubik, S.; Ghosh, B.; Bruzzone, M.J.; Geertz, M.; Martin, V.; Denervaud, N.;
643 Jacquet, P.; Ozkan, B.; Rougemont, J., et al. Two distinct promoter architectures centered on
644 dynamic nucleosomes control ribosomal protein gene transcription. *Genes Dev* **2014**, *28*,
645 1695-1709.
- 646 27. Haruki, H.; Nishikawa, J.; Laemmli, U.K. The anchor-away technique: rapid, conditional
647 establishment of yeast mutant phenotypes. *Molecular cell* **2008**, *31*, 925-932.
- 648 28. Heitman, J.; Movva, N.R.; Hall, M.N. Targets for cell cycle arrest by the immunosuppressant
649 rapamycin in yeast. *Science* **1991**, *253*, 905-909.
- 650 29. Loewith, R.; Hall, M.N. Target of rapamycin (TOR) in nutrient signaling and growth control.
651 *Genetics* **2011**, *189*, 1177-1201.
- 652 30. Miller, S.B.; Ho, C.T.; Winkler, J.; Khokhrina, M.; Neuner, A.; Mohamed, M.Y.; Guilbride, D.L.;
653 Richter, K.; Lisby, M.; Schiebel, E., et al. Compartment-specific aggregases direct distinct
654 nuclear and cytoplasmic aggregate deposition. *Embo J* **2015**, *34*, 778-797.

- 655 31. Thrash, C.; Bankier, A.T.; Barrell, B.G.; Sternglanz, R. Cloning, characterization, and sequence
656 of the yeast DNA topoisomerase I gene. *Proc Natl Acad Sci U S A* **1985**, *82*, 4374-4378.
- 657 32. El Hage, A.; French, S.L.; Beyer, A.L.; Tollervey, D. Loss of Topoisomerase I leads to R-loop-
658 mediated transcriptional blocks during ribosomal RNA synthesis. *Genes Dev* **2010**, *24*, 1546-
659 1558.
- 660 33. French, S.L.; Sikes, M.L.; Hontz, R.D.; Osheim, Y.N.; Lambert, T.E.; El Hage, A.; Smith, M.M.;
661 Tollervey, D.; Smith, J.S.; Beyer, A.L. Distinguishing the roles of Topoisomerases I and II in
662 relief of transcription-induced torsional stress in yeast rRNA genes. *Mol Cell Biol* **2011**, *31*,
663 482-494.
- 664 34. Gallagher, J.E.; Dunbar, D.A.; Granneman, S.; Mitchell, B.M.; Osheim, Y.; Beyer, A.L.; Baserga,
665 S.J. RNA polymerase I transcription and pre-rRNA processing are linked by specific SSU
666 processome components. *Genes Dev* **2004**, *18*, 2506-2517.
- 667 35. Loibl, M.; Klein, I.; Prattes, M.; Schmidt, C.; Kappel, L.; Zisser, G.; Gungl, A.; Krieger, E.;
668 Pertschy, B.; Bergler, H. The drug diazaborine blocks ribosome biogenesis by inhibiting the
669 AAA-ATPase Drg1. *J Biol Chem* **2014**, *289*, 3913-3922.
- 670 36. Krakowiak, J.; Zheng, X.; Patel, N.; Feder, Z.A.; Anandhakumar, J.; Valerius, K.; Gross, D.S.;
671 Khalil, A.S.; Pincus, D. Hsf1 and Hsp70 constitute a two-component feedback loop that
672 regulates the yeast heat shock response. *Elife* **2018**, *7*.
- 673 37. Shi, Y.; Mosser, D.D.; Morimoto, R.I. Molecular chaperones as HSF1-specific transcriptional
674 repressors. *Genes Dev* **1998**, *12*, 654-666.
- 675 38. Zheng, X.; Krakowiak, J.; Patel, N.; Beyzavi, A.; Ezike, J.; Khalil, A.S.; Pincus, D. Dynamic
676 control of Hsf1 during heat shock by a chaperone switch and phosphorylation. *Elife* **2016**, *5*.
- 677 39. Milkereit, P.; Gadal, O.; Podtelejnikov, A.; Trumtel, S.; Gas, N.; Petfalski, E.; Tollervey, D.;
678 Mann, M.; Hurt, E.; Tschochner, H. Maturation and intranuclear transport of pre-ribosomes
679 requires Noc proteins. *Cell* **2001**, *105*, 499-509.

- 680 40. Reiter, A.; Steinbauer, R.; Philippi, A.; Gerber, J.; Tschochner, H.; Milkereit, P.; Griesenbeck, J.
681 Reduction in ribosomal protein synthesis is sufficient to explain major effects on ribosome
682 production after short-term TOR inactivation in *Saccharomyces cerevisiae*. *Molecular and*
683 *cellular biology* **2011**, *31*, 803-817.
- 684 41. Lam, Y.W.; Lamond, A.I.; Mann, M.; Andersen, J.S. Analysis of nucleolar protein dynamics
685 reveals the nuclear degradation of ribosomal proteins. *Curr Biol* **2007**, *17*, 749-760.
- 686 42. Kos-Braun, I.C.; Jung, I.; Kos, M. Tor1 and CK2 kinases control a switch between alternative
687 ribosome biogenesis pathways in a growth-dependent manner. *PLoS Biol* **2017**, *15*,
688 e2000245.
- 689 43. Gomez-Herreros, F.; Rodriguez-Galan, O.; Morillo-Huesca, M.; Maya, D.; Arista-Romero, M.;
690 de la Cruz, J.; Chavez, S.; Munoz-Centeno, M.C. Balanced production of ribosome
691 components is required for proper G1/S transition in *Saccharomyces cerevisiae*. *J Biol Chem*
692 **2013**, *288*, 31689-31700.
- 693 44. Conconi, A.; Paquette, M.; Fahy, D.; Bepalov, V.A.; Smerdon, M.J. Repair-independent
694 chromatin assembly onto active ribosomal genes in yeast after UV irradiation. *Mol Cell Biol*
695 **2005**, *25*, 9773-9783.
- 696 45. Liu, Y.; Liang, S.; Tartakoff, A.M. Heat shock disassembles the nucleolus and inhibits nuclear
697 protein import and poly(A)+ RNA export. *Embo J* **1996**, *15*, 6750-6757.
- 698 46. Tsang, C.K.; Bertram, P.G.; Ai, W.; Drenan, R.; Zheng, X.F. Chromatin-mediated regulation of
699 nucleolar structure and RNA Pol I localization by TOR. *Embo J* **2003**, *22*, 6045-6056.
- 700 47. Mayor, T.; Graumann, J.; Bryan, J.; MacCoss, M.J.; Deshaies, R.J. Quantitative profiling of
701 ubiquitylated proteins reveals proteasome substrates and the substrate repertoire
702 influenced by the Rpn10 receptor pathway. *Mol Cell Proteomics* **2007**, *6*, 1885-1895.
- 703 48. Saarikangas, J.; Barral, Y. Protein aggregates are associated with replicative aging without
704 compromising protein quality control. *Elife* **2015**, *4*.

- 705 49. Tuite, M.F.; Melki, R. Protein misfolding and aggregation in ageing and disease: molecular
706 processes and therapeutic perspectives. *Prion* **2007**, *1*, 116-120.
- 707 50. Cherkasov, V.; Hofmann, S.; Druffel-Augustin, S.; Mogk, A.; Tyedmers, J.; Stoecklin, G.; Bukau,
708 B. Coordination of translational control and protein homeostasis during severe heat stress.
709 *Curr Biol* **2013**, *23*, 2452-2462.
- 710 51. Douglas, P.M.; Treusch, S.; Ren, H.Y.; Halfmann, R.; Duennwald, M.L.; Lindquist, S.; Cyr, D.M.
711 Chaperone-dependent amyloid assembly protects cells from prion toxicity. *Proc Natl Acad Sci*
712 *U S A* **2008**, *105*, 7206-7211.
- 713 52. Grousl, T.; Ungelenk, S.; Miller, S.; Ho, C.T.; Khokhrina, M.; Mayer, M.P.; Bukau, B.; Mogk, A.
714 A prion-like domain in Hsp42 drives chaperone-facilitated aggregation of misfolded proteins.
715 *J Cell Biol* **2018**, *217*, 1269-1285.
- 716 53. Kaganovich, D.; Kopito, R.; Frydman, J. Misfolded proteins partition between two distinct
717 quality control compartments. *Nature* **2008**, *454*, 1088-1095.
- 718 54. Miller, S.B.; Mogk, A.; Bukau, B. Spatially organized aggregation of misfolded proteins as
719 cellular stress defense strategy. *J Mol Biol* **2015**, *427*, 1564-1574.
- 720 55. Decker, C.J.; Parker, R. P-bodies and stress granules: possible roles in the control of
721 translation and mRNA degradation. *Cold Spring Harb Perspect Biol* **2012**, *4*, a012286.
- 722 56. Mahboubi, H.; Stochaj, U. Cytoplasmic stress granules: Dynamic modulators of cell signaling
723 and disease. *Biochim Biophys Acta Mol Basis Dis* **2017**, *1863*, 884-895.
- 724 57. Berry, J.; Weber, S.C.; Vaidya, N.; Haataja, M.; Brangwynne, C.P. RNA transcription modulates
725 phase transition-driven nuclear body assembly. *Proc Natl Acad Sci U S A* **2015**, *112*, E5237-
726 5245.
- 727 58. Feric, M.; Vaidya, N.; Harmon, T.S.; Mitrea, D.M.; Zhu, L.; Richardson, T.M.; Kriwacki, R.W.;
728 Pappu, R.V.; Brangwynne, C.P. Coexisting Liquid Phases Underlie Nucleolar
729 Subcompartments. *Cell* **2016**, *165*, 1686-1697.

- 730 59. Laferte, A.; Favry, E.; Sentenac, A.; Riva, M.; Carles, C.; Chedin, S. The transcriptional activity
731 of RNA polymerase I is a key determinant for the level of all ribosome components. *Genes &*
732 *development* **2006**, *20*, 2030-2040.
- 733 60. Dai, M.S.; Arnold, H.; Sun, X.X.; Sears, R.; Lu, H. Inhibition of c-Myc activity by ribosomal
734 protein L11. *Embo J* **2007**, *26*, 3332-3345.
- 735 61. Liu, Y.; Deisenroth, C.; Zhang, Y. RP-MDM2-p53 Pathway: Linking Ribosomal Biogenesis and
736 Tumor Surveillance. *Trends Cancer* **2016**, *2*, 191-204.
- 737 62. Calo, E.; Flynn, R.A.; Martin, L.; Spitale, R.C.; Chang, H.Y.; Wysocka, J. RNA helicase DDX21
738 coordinates transcription and ribosomal RNA processing. *Nature* **2015**, *518*, 249-253.
- 739 63. Nomura, M. Regulation of ribosome biosynthesis in *Escherichia coli* and *Saccharomyces*
740 *cerevisiae*: diversity and common principles. *J Bacteriol* **1999**, *181*, 6857-6864.
- 741 64. Neef, D.W.; Jaeger, A.M.; Gomez-Pastor, R.; Willmund, F.; Frydman, J.; Thiele, D.J. A direct
742 regulatory interaction between chaperonin TRiC and stress-responsive transcription factor
743 HSF1. *Cell Rep* **2014**, *9*, 955-966.
- 744 65. Mendillo, M.L.; Santagata, S.; Koeva, M.; Bell, G.W.; Hu, R.; Tamimi, R.M.; Fraenkel, E.; Ince,
745 T.A.; Whitesell, L.; Lindquist, S. HSF1 drives a transcriptional program distinct from heat
746 shock to support highly malignant human cancers. *Cell* **2012**, *150*, 549-562.
- 747 66. Santagata, S.; Hu, R.; Lin, N.U.; Mendillo, M.L.; Collins, L.C.; Hankinson, S.E.; Schnitt, S.J.;
748 Whitesell, L.; Tamimi, R.M.; Lindquist, S., et al. High levels of nuclear heat-shock factor 1
749 (HSF1) are associated with poor prognosis in breast cancer. *Proc Natl Acad Sci U S A* **2011**,
750 *108*, 18378-18383.
- 751 67. David, F.P.; Delafontaine, J.; Carat, S.; Ross, F.J.; Lefebvre, G.; Jarosz, Y.; Sinclair, L.;
752 Noordermeer, D.; Rougemont, J.; Leleu, M. HTSstation: a web application and open-access
753 libraries for high-throughput sequencing data analysis. *PLoS One* **2014**, *9*, e85879.

- 754 68. Koplin, A.; Preissler, S.; Ilina, Y.; Koch, M.; Scior, A.; Erhardt, M.; Deuerling, E. A dual function
755 for chaperones SSB-RAC and the NAC nascent polypeptide-associated complex on ribosomes.
756 *J Cell Biol* **2010**, *189*, 57-68.
- 757 69. Tollervey, D.; Lehtonen, H.; Jansen, R.; Kern, H.; Hurt, E.C. Temperature-sensitive mutations
758 demonstrate roles for yeast fibrillarin in pre-rRNA processing, pre-rRNA methylation, and
759 ribosome assembly. *Cell* **1993**, *72*, 443-457.
- 760 70. Beltrame, M.; Tollervey, D. Identification and functional analysis of two U3 binding sites on
761 yeast pre-ribosomal RNA. *Embo J* **1992**, *11*, 1531-1542.
- 762
- 763

Figure Legends

Figure 1: Rapid degradation of Topoisomerase 1 (Top1) induces a transient induction of Heat Shock Factor 1 (Hsf1) target genes and down-regulation of ribosomal protein (RP) genes. (A, B, C) Scatter plots (top panels) and box plots (bottom panels) comparing RNAPII binding (as measured by Rpb1 ChIP-seq) in Top1-AID (A), Top2-AID (B) and Top1/2-AID (C) strains at the indicated times following either auxin or vehicle addition to the media. Indicated gene categories (RP, n=138; ribosome biogenesis [RiBi], n=229; Msn2 target genes, n=45; and Hsf1 target genes, n=19) are color-coded on the scatter plots and displayed separately on the box plots, together with all remaining genes as a fifth class (others, n=4610). (D) Genome browser tracks showing RNAPII (Rpb1) ChIP-seq read counts at the indicated positions on chromosomes X, XIII and VII at 0, 20, or 60 minutes following auxin addition to Top1-AID (top panels) and Top1/2-AID (bottom panel) strains. Gene names and open reading frame (ORF) positions are shown above. (E) Ifh1 occupancy, measured by qPCR ChIP at the *RPL30* and *RPL39* promoters 20 minutes following auxin addition to cultures of Top1-AID and Top1/2-AID strains. Bar height indicates the average and error bars the range of n=4 biological replicates. (F) Schematic representation of protocol for Hsf1-FRB nuclear depletion (anchor-away) induced by rapamycin (Rapa) followed by Top1-AID depletion. (G) Box plots showing RNAPII (Rpb1) ChIP-seq signal following Hsf1-FRB nuclear depletion by anchor-away (-Hsf1, left panel), Top1-AID degradation (auxin, middle panel) or both Hsf1-FRB and Top1-AID depletion (auxin / -Hsf1, right panel) for the five functional groups described in (A).

Figure 2: The effects of Top1 depletion on RNAPII regulation are linked to an underlying defect in ribosome biogenesis. (A) Northern blot of 5'ETS1-containing rRNAs prepared from cultures of wild-type, Top1-AID, Top2-AID and Top1/2-AID cells that had been pulse-labeled for 2 minutes with [³H] adenine at the indicated times following addition of auxin to the media. Total RNAs were extracted and samples were separated on agarose gels, transferred to a nylon membrane and first directly autoradiographed to reveal pulse labelling of nascent rRNAs (see Figure S2A). The membrane was next hybridized with a ³²P-labelled oligonucleotide probe allowing detection of all species containing 5'ETS1 (ACGACAAGCCT-ACTCGAATTCGT). Truncated pre-rRNA fragments, first identified in cells lacking Top1 [32], are indicated (*). (B) Polysome sedimentation profiles (OD₂₆₀) of WT, Top1-AID,

Top2-AID, and Top1/2-AID strains 20 minutes following auxin treatment (large panels, as indicated). The top of each gradient (fractions 7 to 11), corresponding to 40S and 60S subunit peaks, is expanded below, where peak height differences (60S:40S ratio) are indicated. (C) Total cell extracts prepared from the indicated fractions of sedimentation profiles of WT and Top1/2-AID strains (from B) were TCA precipitated and analyzed by Western blot following SDS-PAGE, using an antibody against Rpl3 and Rps8, as indicated. (D) Total (left panels) and detergent-insoluble pellet (right panels) fractions isolated from lysates of Top1/2AID cells treated (+) or not (-) with auxin were analyzed by SDS-PAGE and Coomassie blue staining (top panels) or immunoblotting with the indicated antibodies (bottom panels). The pellet fraction is overloaded 25-fold compared to the total extract fractions. (E, F, G) Scatter plots (top panels) comparing RNAPII (Rpb1) ChIP-Seq read counts for individual genes in Utp8-AID (E) or Utp13-AID (F) cells after 20 minutes of auxin or vehicle treatment, or WT cells after 20 minutes of treatment with diazaborine or vehicle (G) (y-axis: auxin or diazaborine) for 20 minutes versus non-depleted cells (x-axis, Vehicle). Each dot represents a gene (5,041 genes in total) and genes are color-coded according to functional groups, as in Figure 1A. Bottom panels display the corresponding box plots for the four indicated gene categories plus all other genes (others).

Figure 3: Evidence that Ifh1 is rapidly removed from RP gene promoters and sequestered in an insoluble nucleolar fraction pursuant to unassembled RP accumulation following RASTR initiation.

(A) Ifh1 occupancy at the *RPL30* and *RPL37A* promoters 20 minutes following vehicle, rapamycin or auxin treatment of Top1/2-AID strains expressing either WT Ifh1 (*IFH1*) or a C-terminal truncated allele (*ifh1-ΔC*). Bar height indicates the average and error bars the range of N=4 biological replicates. (B) Box plots showing the kinetics of RNAPII ChIP-seq changes at Hsf1 target and RP genes at the indicated time points (minutes) following auxin treatment in Top1/2-AID (top panel) or Top1-AID (bottom panel) strains. (C) A Top1/2-AID strain expressing Ifh1-eGFP and Nhp6-mCherry was grown exponentially and cell samples were used for fluorescence microscopy analysis after 20 minutes of auxin (Aux) or vehicle (Veh) treatment. (D) *TOM1* (top panels) and *tom1-Δ* (bottom panels) strains expressing Ifh1-eGFP and Nhp6-mCherry were grown exponentially and cell samples were used for fluorescence or transmission microscopy analysis, as indicated. (E) 10-fold serial dilutions of *IFH1*, *ifh1-AA* (*ifh1 680A/681A*) or *ifh1-6* cells transformed in either *TOM1* or *tom1-Δ* backgrounds (as

indicated) were grown in YPD medium for 44 hours at 30°C before being photographed. (F) Scatter plot comparing average number of peptides purified in an insoluble fraction from Top1/2-AID cells treated for 20 minutes with either auxin (y-axis, Auxin) or vehicle (x-axis, Vehicle). Each dot represents a protein, color-coded according to functional group as above (green: RP, red: Hsf1 target gene product, yellow: RiBi protein, grey: others), with some specific proteins indicated by arrows. (G) Gene Ontology and p-values of protein groups that are the most enriched in the insoluble fraction following Top1/2-AID depletion ($\Delta > 3$ peptides in insoluble fraction after topoisomerase depletion compared to vehicle in all experiments, n=3 biological replicates).

Figure 4: Down-regulation of RP gene expression by Ifh1 nuclear depletion prior to RASTR initiation

strongly dampens Hsf1 target gene activation. (A) Schematic of protocol for Ifh1-FRB nuclear depletion (0-60 minutes of rapamycin treatment) followed by Top1-AID or Top1/2-AID degradation (auxin treatment, 40-60 min). (B) Scatter plot comparing RNAPII (Rpb1) ChIP-seq in Ifh1-FRB cells either rapamycin-treated for 60 min (y-axis, -Ifh1, Ifh1-FRB nuclear depletion) or un-treated (x-axis, Vehicle, no Ifh1-FRB depletion). Categorization and color-coding of genes as above. (C) Northern blots of pre-rRNA after 0 or 60 minutes of Ifh1-FRB nuclear depletion by anchor-away (-Ifh1) or vehicle (Veh) treatment of Ifh1-FRB strain. (D) Box plots of the data shown in (B) for the indicated five gene categories, showing fold-change upon Ifh1-FRB nuclear depletion compared to mock treated cells. (E) Scatter plots comparing RNAPII (Rpb1) ChIP-seq in Top1-AID Ifh1-FRB cells either auxin-treated (y-axis, Aux, left panel) or auxin- plus rapamycin-treated (y-axis, Aux / -Ifh1, right panel) treated, as described in (A), versus untreated cells (x-axis, vehicle, both panels). (F) As in (E), but for Top1/2-AID Ifh1-FRB cells. (G) Box plots showing RNAPII (Rpb1) ChIP-seq change after rapamycin and/or auxin treatment for Hsf1 target genes in Top1-AID Ifh1-FRB cells (left) or Top1/2-AID Ifh1-FRB cells (right). Asterisks show significant difference according to student's t-test (*: $p < 0.05$, ***: $p < 0.001$, ns: Not significant), p-value is indicated.

Figure 5: Cycloheximide treatment induces a rapid RNAPII transcriptional response opposite and

epistatic to that of RASTR. (A) Schematic related to experiments in subsequent panels describing the effect of cycloheximide treatment on *de novo* RP production and auxin treatment on Top1-AID (or Top1/2-AID) degradation. (B) Northern blots of pre-rRNA after 0, 5, 10, and 20 minutes of

cycloheximide (CHX) treatment. **(C)** Scatter plot comparing RNAPII (Rpb1) ChIP-seq after 20 minutes of cycloheximide treatment (y-axis, CHX) to that of non-treated cells (x-axis, vehicle) at the indicated groups of target genes. **(D)** Scatter plots comparing RNAPII ChIP-seq in auxin-treated to untreated cells (left panel) and in auxin + cycloheximide (CHX)-treated to untreated cells (right panel). In both cases cells express Top1-AID. **(E)** Scatter plots comparing RNAPII ChIP-seq as in (D), but for Top1/2-AID cells. **(F)** Box plots showing RNAPII ChIP-seq fold-change for Hsf1 target genes after cycloheximide (CHX) and/or auxin (Aux) treatment of Top1-AID or Top1/2-AID cells, as indicated (data taken from experiments shown in (D) and (E)). P-values are shown above the indicated comparisons together with significance according to student's t-test (***: $p < 0.001$, ns: not significant). **(G-H)** Top1/2-AID strains expressing Rpl25-eGFP **(G)** or Ifh1-eGFP **(H)** and Nhp6-mCherry were grown exponentially and samples were used for fluorescence microscopy analysis after 20 minutes of auxin (top) or vehicle treatment (bottom), in the absence (left) or presence (right) of cycloheximide (CHX).

Figure 6: RASTR comprises the cycloheximide-sensitive component of the early RNAPII response to TORC1 inhibition. **(A)** Northern blots of pre-rRNA from wild type cells after 5 or 30 minutes of vehicle (Veh) or rapamycin (Rap) treatment. **(B)** Scatter plots comparing RNAPII (Rpb1) ChIP-seq in cells after 5 (y-axis, left panel) or 20 minutes (y-axis, right panel) of rapamycin (Rap) treatment to non-treated cells (x-axis, vehicle). Gene groups are color-coded as indicated. **(C)** Genome browser tracks showing RNAPII ChIP-seq read counts for three consecutive RP genes on chromosome X (in green, left panel) or at the *SSA1* gene on chromosome I (in red, right panel), following 0, 5, or 20 min (top, middle, bottom panels, respectively) of rapamycin treatment. Gene annotations (gene name, open reading frame and direction of transcription) are shown above the tracks. **(D)** Scatter plots comparing RNAPII ChIP-seq in cells pre-treated with cycloheximide (CHX) then treated for 5 (left panel) or 20 (right panel) minutes with rapamycin to cells untreated (x-axis, vehicle). Schematic representation of the experimental protocols is shown below each panel. Cells were collected for RNAPII ChIP-seq analysis after 5 (left panel) or 20 minutes (right panel) of rapamycin treatment. **(E)** Ifh1 occupancy at the *RPL30* and *RPL37A* promoters following 5 or 20 minutes of rapamycin treatment (Rap) in cells pre-treated or not with cycloheximide (CHX) for 5 minutes. Bar height indicates the average and error bars the range of N=4 biological replicates.

Figure 7: RP gene down-regulation following heat shock is blocked by cycloheximide. (A) Scatter plots comparing RNAPII ChIP-Seq in cells pre-treated or not with cycloheximide (CHX) followed by 5 minutes of heat shock (y-axis, HS) versus non-stressed cells (x-axis, no HS, no CHX). Schematic of the protocol for each experiment is shown below the data panels: mock pre-treatment (vehicle; 0-5 min) followed by heat shock (HS; 40°C, 5-10 min; left panel) or cycloheximide (CHX) pre-treatment (0-5 min) followed by heat shock (HS; 40°C, 5-10 min; right panel). Samples for ChIP-seq analysis of RNAPII association were taken at 10 minutes in both experiments. (B, C) Genome browser tracks showing RNAPII ChIP-Seq read counts for the experiments described in (A) on a region on chromosome X containing three consecutive RP genes (in green, (B)) or at the *SSA1* gene on chromosome I (in red, (C)). Cells were either mock pre-treated (vehicle; left panels) or cycloheximide pre-treated (CHX; right panels) before heat shock (HS). Gene annotations (gene name, open reading frame and direction of transcription) are shown above the tracks.

Figure 8: RP and Hsf1 target genes are regulated as a function of unassembled RP levels in both growing and stressed cells. In rapidly-growing, un-stressed cells, RNAPII initiation at RP and Hsf1 target genes is continuously adjusted according to the levels of un-assembled RPs (central sector). Under various stress conditions (including RASTR, heat shock, TORC1 inhibition, perhaps many others) levels of unassembled RPs increase dramatically, and RPs accumulate with nucleolar proteins, Ifh1 and chaperones in an insoluble nuclear or nucleolar fraction. This leads to the rapid up-regulation of Hsf1 target genes (e.g. chaperones and proteasome components), presumably through Hsp70 titration, and to the coincident down-regulation of RP genes, through Ifh1 sequestration (bottom left sector, “RP excess”). Conversely, a decrease in RP production (as provoked here by cycloheximide treatment) will lead to an opposite transcriptional response (bottom right sector, “RP depletion”). In summary, we propose that levels of unassembled nuclear RPs act to constantly adjust RP and Hsf1 target gene expression, allowing the cell to balance growth with protein homeostasis.

Supplementary Figure legends

Figure 1- figure supplement 1. (A) 10-fold serial dilution of Top1-AID or Top1/2-AID cells spotted onto rich medium and grown at 30°C for 24 or 48 hours with or without auxin treatment. (B) Top1 or Top2 tagged as indicated were detected by Western blot using antibodies against Myc or AID antibody in a whole cell extract. Ponceau red stain served as a loading control (bottom panel). (C) GO of genes that are upregulated (Rpb1-ChIP) more than two times following Top1 depletion. (D) Circle diagram showing number of RP genes in the 146 genes downregulated more than two times following Top1 depletion. (E-F) Rap1 (E) or Fhl1 (F) occupancy at the *RPL30* and *RPL39* promoters at 20 min following Top1 or Top1/2 depletion. (G) 10-fold serial dilution of anchor away cells background spotted onto rich medium and grown at 30°C for 40 hours with (Auxin, Rapamycin) or without treatment (vehicle).

Figure 2- figure supplement 1. (A) A Top1/2-AID strain expressing Btn2-eGFP and Nop1-mCherry was grown to exponential phase and cell samples were used for fluorescence microscopy analysis after 20 min of vehicle (Veh) treatment (mock depletion; top panels) or auxin (Aux) treatment (Top1/2 depletion; bottom panels). The number of Btn2-eGFP foci per cell was quantified and is presented in the panel to the right. 75–100 cells were quantified for each experiment, and the data are reported as averages from two experiments, with standard deviations indicated. (B) A Top1/2-AID strain expressing Pre6-eGFP and Nop56-mCherry was grown exponentially and cell samples were used for fluorescence microscopy analysis after 20 min of Top1/2 depletion by auxin treatment (Aux) or mock depletion (Veh). The number of cells where Pre6-eGFP showed a peri-nuclear localization was quantified and is presented as a percentage. 75–100 cells were quantified for each experiment, and the data are reported as averages from two experiments, with standard deviations indicated. (C) Yeast cells (either wild type, Top1-AID, Top2-AID or Top1/2-AID, as indicated) were grown synthetic glucose medium lacking adenine to mid-log phase at which point auxin was added (to 0.5mM) and cells were then pulse labeled with [³H] adenine for 2 minutes at different time points after auxin addition (T=0, 10, 20, 30 min). RNAs were extracted and samples were separated on agarose gels, transferred to a nylon membrane. After documenting ³H labelling by autoradiography, the same

membrane was used for the Northern blot shown in Figure 2A. (D) RNAPII ChIP occupancy at the *RPL30* and *RPL39* promoters or at the *SSA4* and *HSP42* promoters at 20 minutes following Top1 and Top2 depletion.

Figure 3- figure supplement 1. (A) Scatter plot comparing iBAQ abundances (Δ -iBAQ: intensity-Based Absolute Quantification) of peptides recovered from an insoluble fraction of bortezomib-treated wild type (x-axis) or *tom1- Δ* cells (y-axis). Each dot represents a protein, color-coded according to functional group as above (green: RP, red: Hsf1 target gene product, yellow: RiBi protein, grey: others), with some specific proteins indicated by arrows. Raw data are from [13,14]. **(B)** Box plot showing number of peptides corresponding to large (RPL) or small (RPS) ribosomal proteins recovered from insoluble fraction in cells treated for 20 minutes with either auxin (Aux) or vehicle (Veh).

Figure 4- figure supplement 1. (A) 10-fold serial dilution of anchor away cells background spotted onto rich medium and grown at 30°C for 40 hours with (Auxin, Rapamycin) or without treatment (vehicle). **(B)** Average Ifh1 ChIP-seq signal related to the TSS at promoters of RP or Hsf1 genes.

Figure 5- figure supplement 1. (A) Box plots showing RNAPII ChIP-seq fold-change for Hsf1 target genes after auxin (Aux) and/or cycloheximide (CHX) treatment of Top1-AID or Top1/2-AID cells, as indicated. **(B)** A *tom1- Δ* strain expressing Ifh1-eGFP and Nhp6-mCherry was grown to mid-exponential phase and cell samples were used for fluorescence microscopy analysis following 20 min of vehicle (top panels) or cycloheximide (CHX; bottom panels) treatment. **(C)** Ifh1 occupancy at the *RPL30* promoter 20 min following cycloheximide (CHX, red) or vehicle (Veh, blue) treatment in wild type (*TOM1*) or *tom1- Δ* cells. **(D)** Ifh1 occupancy at the *RPL30* and *RPL37A* promoters 0 or 20 min following mock or Top1/2-AID depletion (- or Aux) in the presence (CHX) or absence (-) of cycloheximide. **(E, F)** Numbers of cells where Rpl25-eGFP (E) or Ifh1-eGFP (F) nuclear foci were identified, presented as a percentage. In each experiment 75–100 cells were used for the

955 quantification. Data are reported as averages from two experiments, with standard deviations
956 indicated.
957

Supplementary files

Supplementary File 1. Rpb1 ChIP-seq at the indicated times following either auxin or vehicle addition to the media in Top1-AID, Top2-AID or Top1-AID Top2-AID strain.

Supplementary File 2. Rpb1 ChIP-seq at the indicated times following either auxin (Aux), vehicle (veh), diazaborine (Diaz), or cycloheximide (CHX) addition to the media.

Supplementary File 3. Number of peptides purified in an insoluble fraction from Top1/2-AID cells treated for 20 minutes with either auxin or vehicle.

Supplementary File 4. Rpb1 ChIP-seq in Top1-AID Ifh1-FRB or Top1-AID Top2-AID Ifh1-FRB cells following either auxin, auxin plus rapamycin, or rapamycin addition to the media.

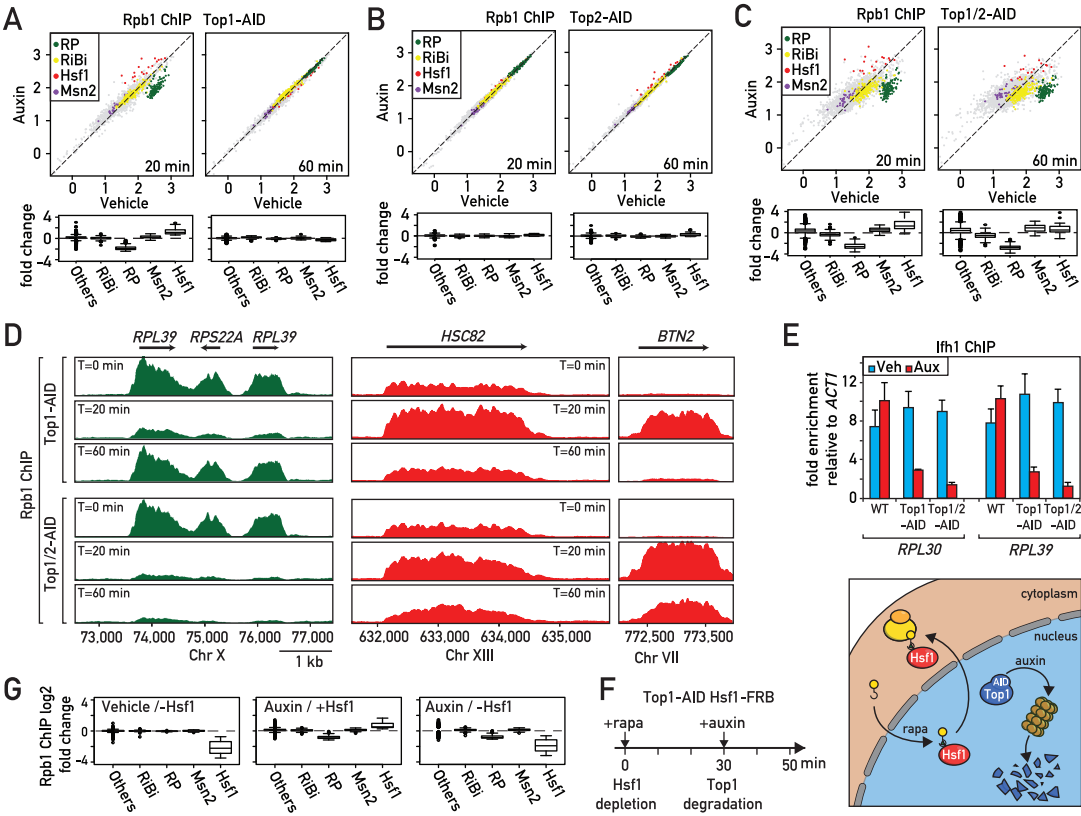
Supplementary File 5. Rpb1 ChIP-seq in Top1-AID or Top1/2-AID cells following either auxin, auxin plus cycloheximide, or vehicle addition to the media.

Supplementary File 6. Rpb1 ChIP-seq in wild type cells following either Vehicle (Veh) or Rapamycin (Rap) addition, Cycloheximide pre-treatment (CHX), or Heat Shock at 40°C (Heat Shock).

Supplementary File S7. Yeast strains used in this study.

Supplementary File 8. DNA Primers used in this study.

Figure 1



A

WT Top1-AID Top2-AID Top1/2-AID min

0 10 20 30 0 10 20 30 0 10 20 30 0 10 20 30

35S

23S

*

*

B

WT Top1-AID

80S polysome

10 15 20

35 60S 5.48

7 9 11

Top2-AID Top1/2-AID

10 15 20

3.9

7 9 11

C

input gradient top 40S 60S 80S polysome

WT

ab Rpl3

ab Rps8

Top1/2-AID

ab Rpl3

ab Rps8

fraction 1 2 3 4 5 6 7 8 9 10 11 12 13 14 15 16

D

Top1/2-AID

total(1x) insoluble(25x)

Auxin - + - + - + - +

Coomassie

Rpl6

Rpl3

Act1

KDa

130

100

70

55

35

25

15

E

Rpb1 ChIP

Auxin

RP

RiBi

Hsf1

Msn2

Utp8-AID

Vehicle

fold change

Others

RiBi

RP

Msn2

Hsf1

F

Rpb1 ChIP

Auxin

RP

RiBi

Hsf1

Msn2

Utp13-AID

Vehicle

fold change

Others

RiBi

RP

Msn2

Hsf1

G

Rpb1 ChIP

Diazaborine

RP

RiBi

Hsf1

Msn2

WT

Vehicle

fold change

Others

RiBi

RP

Msn2

Hsf1

Figure 3

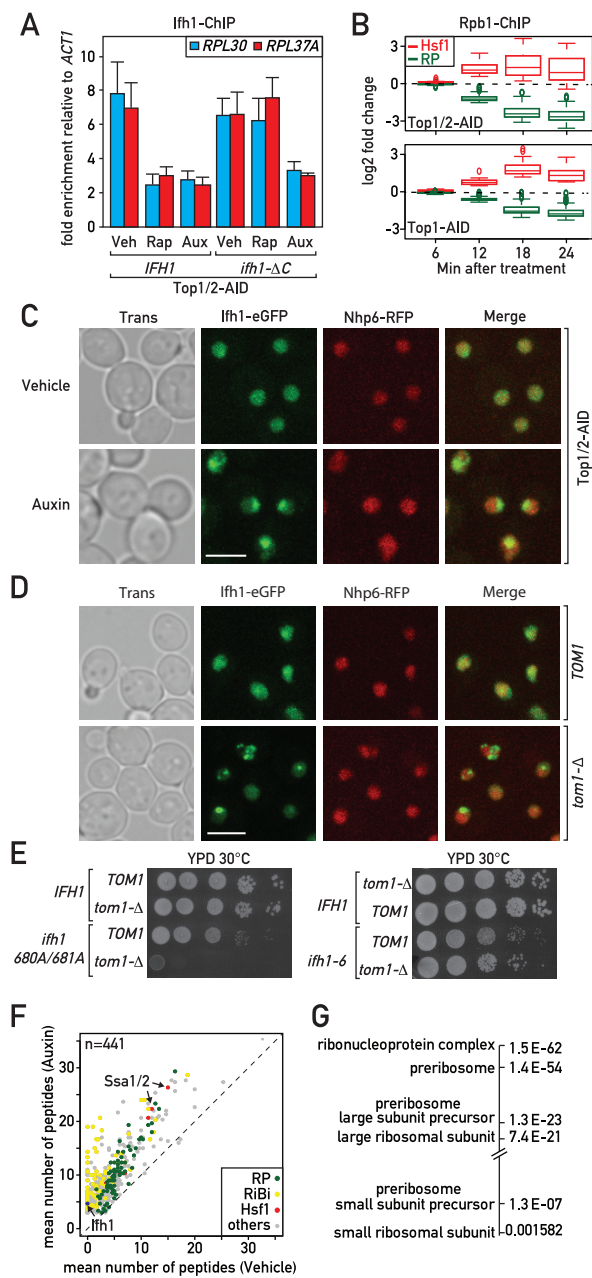


Figure 4

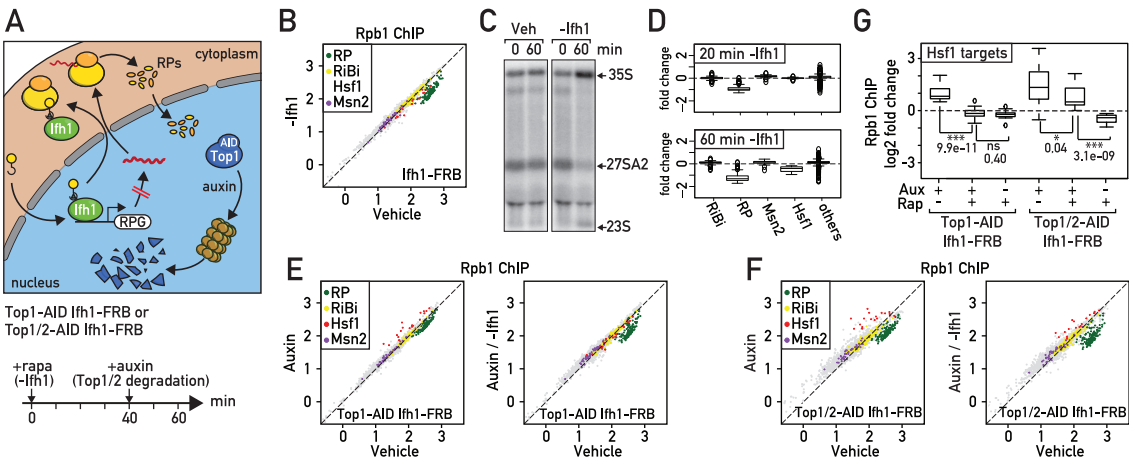


Figure 5

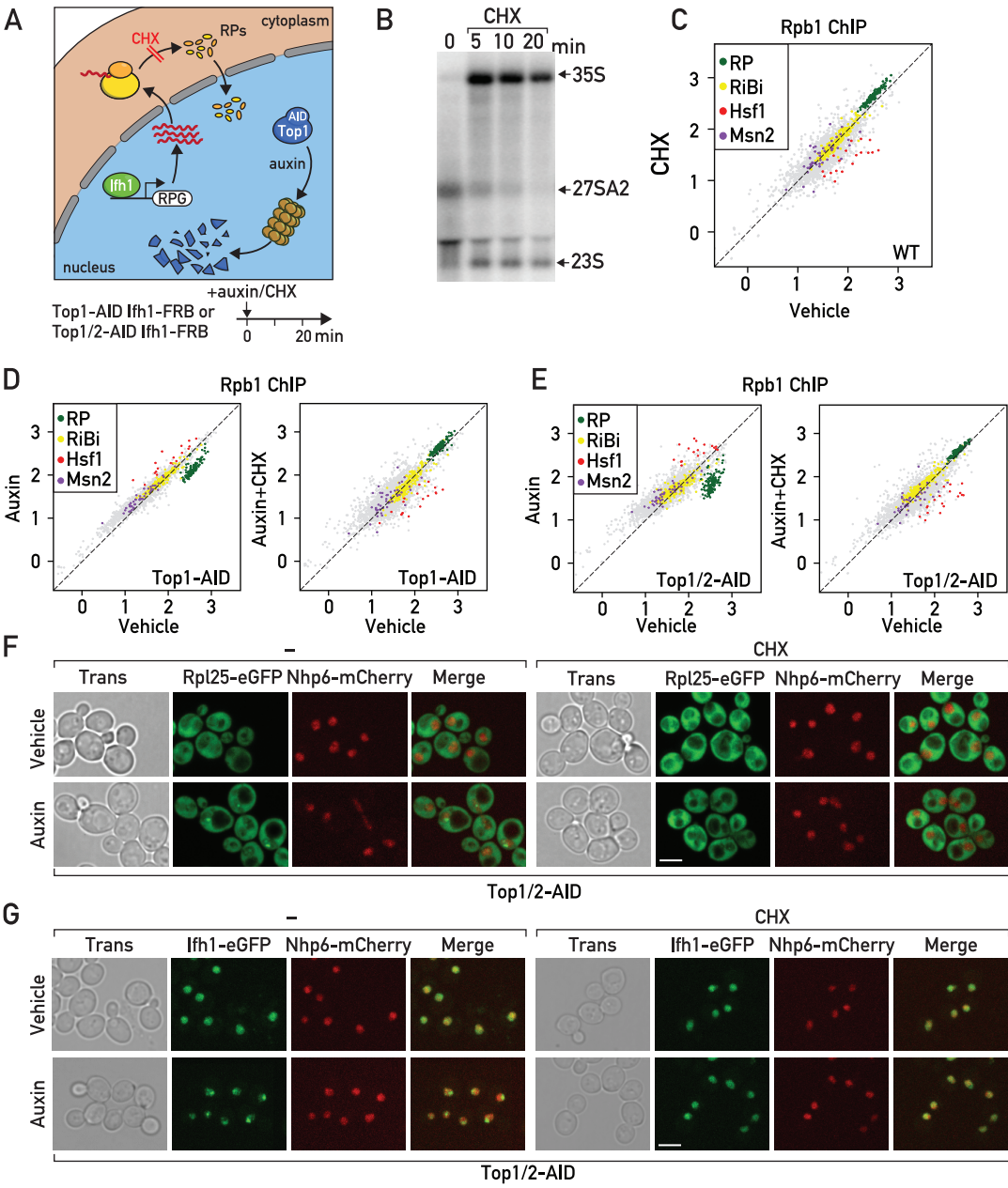


Figure 6

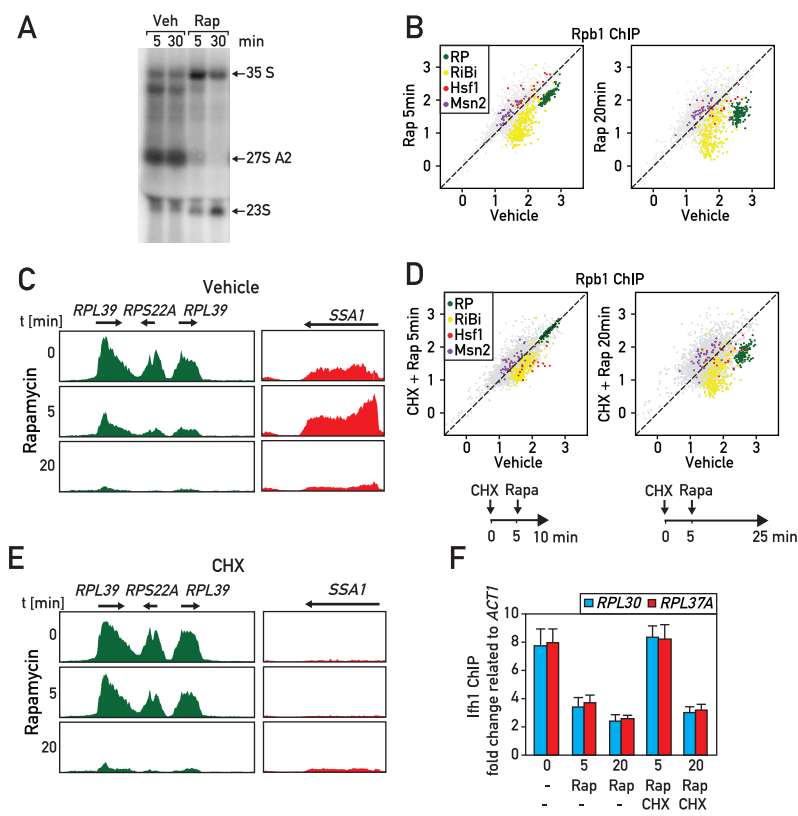


Figure 7

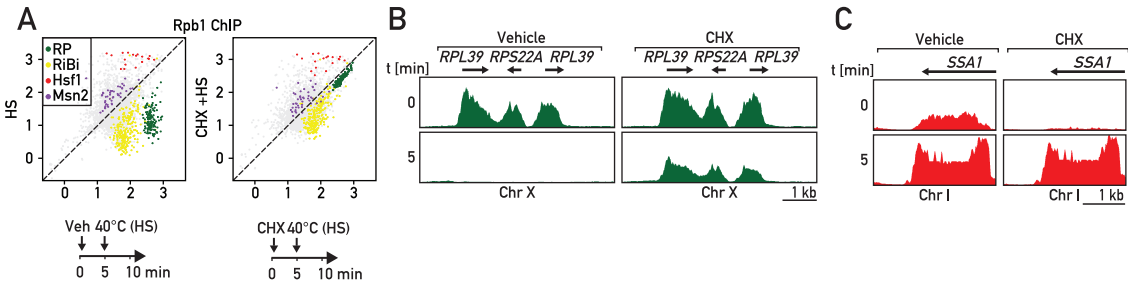
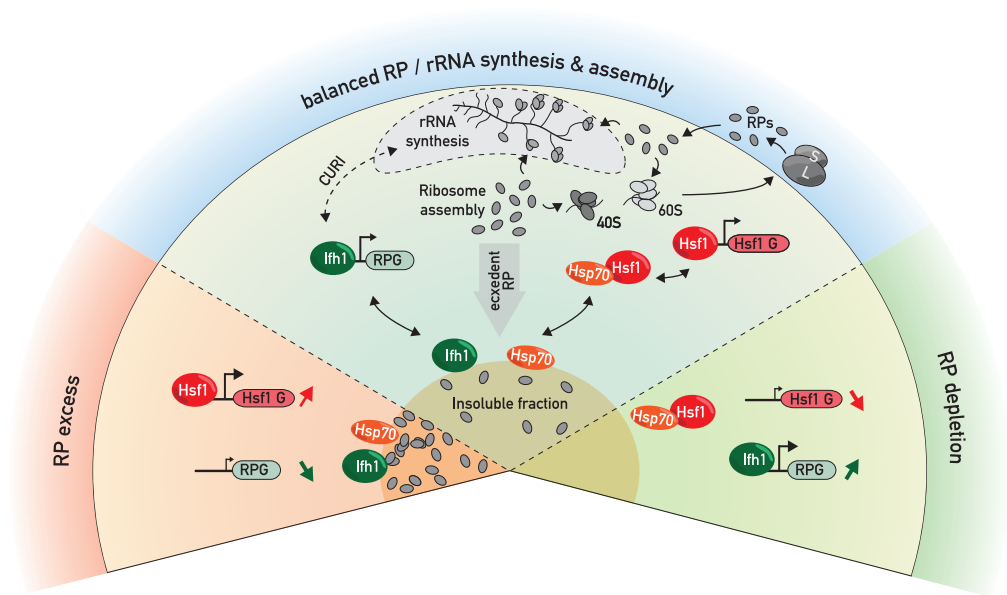
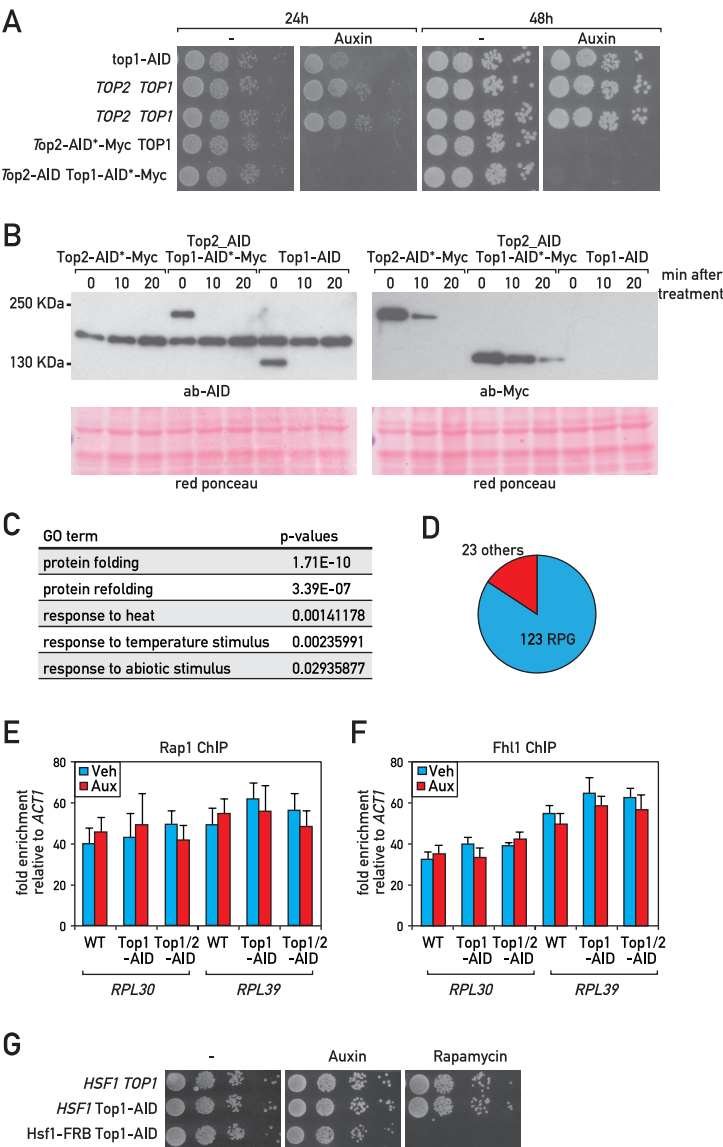


Figure 8

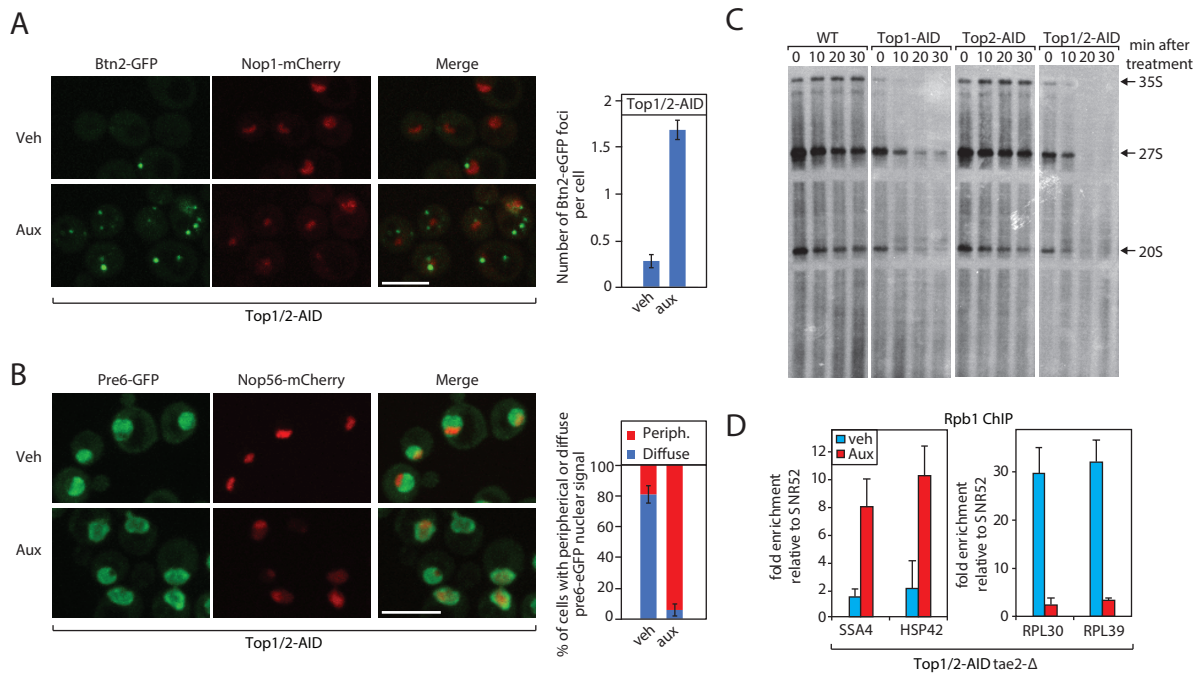


Supplemental Figure S1



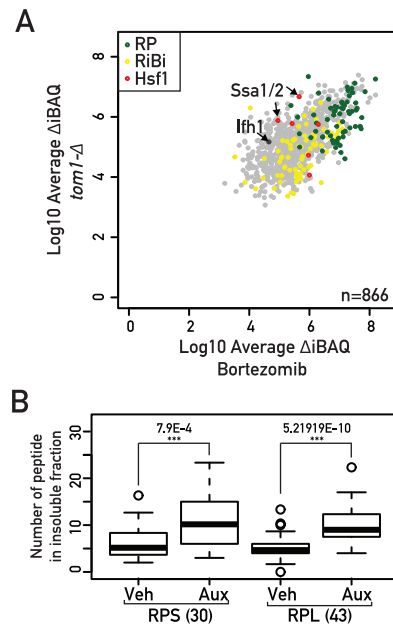
Supplementary Figure S1: Data related to Figure 1. (A) 10-fold serial dilution of Top1-AID or Top1/2-AID cells spotted onto rich medium and grown at 30°C for 24 or 48 hours with or without auxin treatment. (B) Top1 or Top2 tagged as indicated were detected by Western blot using antibodies against Myc or AID antibody in a whole cell extract. Ponceau red stain served as a loading control (bottom panel). (C) GO of genes that are upregulated (Rpb1-ChIP) more than two times following Top1 depletion. (D) Circle diagram showing number of RP genes in the 146 genes downregulated more than two times following Top1 depletion. (E-F) Rap1 (E) or Fhl1 (F) occupancy at the *RPL30* and *RPL39* promoters at 20 min following Top1 or Top1/2 depletion. (G) 10-fold serial dilution of anchor away cells background spotted onto rich medium and grown at 30°C for 40 hours with (Auxin, Rapamycin) or without treatment (Vehicle).

Supplemental Figure S2



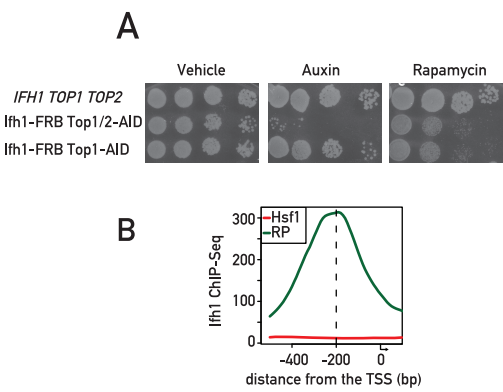
Supplementary Figure S2: Data related to Figure 2. (A) A Top1/2-AID strain expressing Btn2-eGFP and Nop1-mCherry was grown to exponential phase and cell samples were used for fluorescence microscopy analysis after 20 min of vehicle (Veh) treatment (mock depletion; top panels) or auxin (Aux) treatment (Top1/2 depletion; bottom panels). The number of Btn2-eGFP foci per cell was quantified and is presented in the panel to the right. 75–100 cells were quantified for each experiment, and the data are reported as averages from two experiments, with standard deviations indicated. (B) A Top1/2-AID strain expressing Pre6-eGFP and Nop56-mCherry was grown exponentially and cell samples were used for fluorescence microscopy analysis after 20 min of Top1/2 depletion by auxin treatment (Aux) or mock depletion (Veh). The number of cells where Pre6-eGFP showed a peri-nuclear localization was quantified and is presented as a percentage. 75–100 cells were quantified for each experiment, and the data are reported as averages from two experiments, with standard deviations indicated. (C) Yeast cells (either wild type, Top1-AID, Top2-AID or Top1/2-AID, as indicated) were grown synthetic glucose medium lacking adenine to mid-log phase at which point auxin was added (to 0.5mM) and cells were then pulse labeled with [³H] adenine for 2 minutes at different time points after auxin addition (T=0, 10, 20, 30 min). RNAs were extracted and samples were separated on agarose gels, transferred to a nylon membrane. After documenting ³H labelling by autoradiography, the same membrane was used for the Northern blot shown in Figure 2A. (D) RNAPII ChIP occupancy at the *RPL30* and *RPL39* promoters or at the *SSA4* and *HSP42* promoters at 20 minutes following Top1 and Top2 depletion.

Supplemental Figure S3



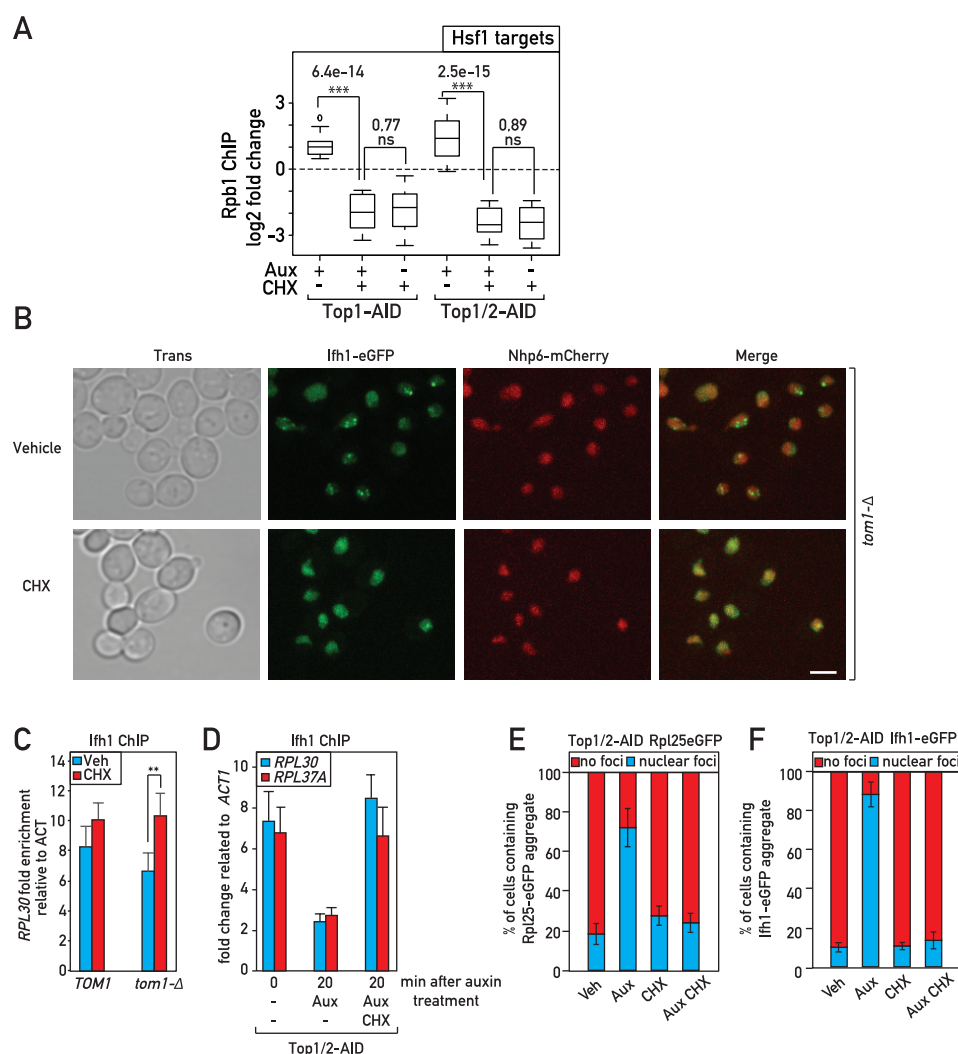
Supplementary Figure S3: Data related to Figure 3. (A) Scatter plot comparing iBAQ abundances (Δ -iBAQ: intensity-Based Absolute Quantification) of peptides recovered from an insoluble fraction of bortezomib-treated wild type (x-axis) or *tom1-Δ* cells (y-axis). Each dot represents a protein, color-coded according to functional group as above (green: RP, red: Hsf1 target gene product, yellow: RiBi protein, grey: others), with some specific proteins indicated by arrows. Raw data are from [13,14]. (B) Box plot showing number of peptides corresponding to large (RPL) or small (RPS) ribosomal proteins recovered from insoluble fraction in cells treated for 20 minutes with either auxin (Aux) or vehicle (Veh).

Supplemental Figure S4



Supplementary Figure S4: Data related to Figure 4. (A) 10-fold serial dilution of anchor away cells background spotted onto rich medium and grown at 30°C for 40 hours with (Auxin, Rapamycin) or without treatment (vehicle). (B) Average Ifh1 ChIP-seq signal related to the TSS at promoters of RP or Hsf1 genes.

Figure 5-figure supplement 1



Supplementary Figure S5: Data related to Figure 5. (A) Box plots showing RNAPII ChIP-seq fold-change for Hsf1 target genes after auxin (Aux) and/or cycloheximide (CHX) treatment of Top1-AID or Top1/2-AID cells, as indicated. (B) A *tom1-Δ* strain expressing Ifh1-eGFP and Nhp6-mCherry was grown to mid-exponential phase and cell samples were used for fluorescence microscopy analysis following 20 min of vehicle (top panels) or cycloheximide (CHX; bottom panels) treatment. (C) Ifh1 occupancy at the *RPL30* promoter 20 min following cycloheximide (CHX, red) or vehicle (Veh, blue) treatment in wild type (*TOM1*) or *tom1-Δ* cells. (D) Ifh1 occupancy at the *RPL30* and *RPL37A* promoters 0 or 20 min following mock or Top1/2-AID depletion (- or Aux) in the presence (CHX) or absence (-) of cycloheximide. (E, F) Numbers of cells where Rpl25-eGFP (E) or Ifh1-eGFP (F) nuclear foci were identified, presented as a percentage. In each experiment 75–100 cells were used for the quantification. Data are reported as averages from two experiments, with standard deviations indicated.